

Authors answers to tc-2019-210 comments

March 28th, 2020

Dear Editor,

We are pleased to submit the revised manuscript of our paper entitled “Landfast sea ice material properties derived from ice bridge simulations using the Maxwell Elasto-Brittle rheology” by Mathieu Plante, Bruno Tremblay, Martin Losch and Jean-François Lemieux.

We would like to thank the reviewers for their useful comments and suggestions. We have modified our manuscript according to most suggestions of the reviewers. This helped improve the clarity of the article substantially. Note that the title of the manuscript was also changed, as suggested by Referee #2.

Thank you for your consideration for publication.

Sincerely,

On behalf of all the authors,
Mathieu Plante

Note :

- The referee comments are shown in black,
- The authors answers are shown in blue,
- *Quoted texts from the revised manuscript are shown in italic and in dark blue.*

Answers to tc-2019-2010 RC1

March 28th, 2020

Note :

- The referee comments are shown in black,
- [The authors answers are shown in blue,](#)
- *Quoted texts from the revised manuscript are shown in italic and in dark blue.*

The manuscript named “The material properties of ice bridges in the Maxwell Elasto-Brittle rheology” test the MEB sea-ice rheology in a traditional finite difference framework. The aim is to investigate the damage parameterisation. This is achieved with an idealized model setup of a channel that is narrow in the middle and wider in the two ends. I think that this is a very relevant to study the damage parameterisation as this (at least in my opinion) is important for new developments within sea-ice dynamics. The manuscript is in general well written and therefore fairly easy to read.

I could wish for a better organization of the figures. In addition, the result section would be much easier to read if the figures were numbered in the order they are referenced. At last I think that the simplifications made in terms of zero ocean currents/sea surface tilt may have bigger impact, especially in some of the examples mentioned within the Canadian archipelago, where tides are significant. This is not necessary to include within this study but a better discussion of the limitation would be nice.

The results in general seems less impressive than other studies using the MEB rheology. A discussion of the performance of these would also be nice. Many of these points are mentioned but I think that it would be beneficial to collect these in a discussion and maybe spend a few more words.

[We thank the referee for his or her thorough review of the manuscript and constructive comments.](#)

Major revisions:

I think that the focus of the abstract is a bit off and I would like this to be revised. It is not that important that the framework of the sea-ice model originally was build for VP dynamics as this is not mentioned in the manuscript. The eulerian/lagrangian implementation is more relevant. I would like the abstract to include line 77-82 as these fit well into a summary/abstract and less into the introduction. Corrected as suggested by the reviewer

>> [As suggested by the reviewer, the abstract was re-written to better reflect the manuscript's content.](#)

We have kept however the sentence about the implementation of the MEB model on the Eulerian, finite differentiation framework, because this allows for a direct comparison with other models commonly used in GCMs. This is not a trivial task and many have tried without success. This is considered a significant contribution for the ice modeling community that is worth reporting in the abstract. Instead, we have put more emphasis on this in the body of the paper to justify its inclusion in the abstract.

Discussions are scattered around in the manuscript. I would like a collected discussion.

>> We added a new section where we collected our discussions on the damage parameterization, its instabilities and the orientation of the lines of fractures.

- What improvements/limitations are there when the framework moves from a Lagrangian to an Eulerian approach.

>> The limitations of moving from a Lagrangian to a Eulerian framework is mainly linked with the advection of tracers within the model. A Lagrangian approach allows to follow deforming elements within the domain resulting in low numerical diffusion. The disadvantage of this approach is that one must recalculate a new grid periodically (called regridding) when the elements are too distorted, requiring the use of interpolation techniques that leads to diffusion of resolved features and requiring a significant amount of CPU time. In a Eulerian framework, higher order advection schemes are typically used (but not here) to limit numerical diffusion and the model grid remains the same throughout the full integration, resulting in lower CPU cost. Note also that the use of a Eulerian scheme is not novel here: the MEB model was originally implemented in a Eulerian scheme in Dansereau et al., 2016, although using Finite Element Methods.

The goal here is not so much about model improvements (or limitations), but rather about advantages of having two different models on the same platform. This has been clarified at L218-221 in the revised manuscript. Namely, the advantages of coding the MEB model using a Eulerian, finite differentiation framework is that it allows for a direct comparison of the MEB model physics (rheology, yield curve, deformations) with that of the standard viscous plastic approach (or variation thereof) used in the vast majority of GCMs and coupled ice-ocean models, independently of the differences in the numerical framework (i.e. Lagrangian vs Eulerian advection scheme, regridding, the use of Finite Element Methods and triangular mesh). The caveats of using the Finite Difference scheme is also discussed in section 2.3.2, at L263-279.

The study limits the effects of the ocean (eg. tides) by neglecting it. For an idealized study like this it is fine just to look at the wind. But in terms of comparisons with real data then this restricts the value of the study. Tides are very high from Kanes Basin and southwards. This is an important factor when the stability of the last fast ice is to be considered and compared with real life. This is briefly mentioned on line 500, however I would like a bigger discussion of this.

>> We agree with the reviewer that the tides and thermal stresses are important in the landfast ice break up process. Here, we consider our “wind forcing” to be representative of the combined surface forces on the ice from both winds and ocean currents including tides, which vary depending on the location. This was clarified in the revised manuscript by re-writing the surface forcing into a landfast ice forcing term independent of the ice velocity and a water drag term that is only significant in drifting ice. As such, the forcing imposed on the ice bridge is no longer assumed to originate from the winds. The simulations are now discussed in terms of forcing values, rather than wind magnitude. Note that our ideal simulations and cohesion estimates are not sensitive to the source of the forcing, only to its

magnitude and direction. This is now clarified at L86-L96. The wind forcing and surface current values associated to the forcing used to derive the material properties of sea ice is also indicated at L402-403. We believe that a lengthy discussion on these factors is outside of the scope of this paper, which is concerned with the simulation of ice arches in the MEB framework and the influence of the material properties in their formation and stability. We also clarified the scope of the study in the introduction so as to not create expectations that are not met in the body of the paper.

Figures are very inconsistent when labeling. These should be changed. I have suggested updates to almost all of the figures. These comments are in the minor correction/technical correction part.

>> There was a duplicated figure in the manuscript that led to confusion in the automatic latex-referencing. This addressed several of the comments raised by the reviewer. We apologize for not noticing this before submission. We have corrected all other issues as proposed by the reviewer.

Minor details

Line 2- Please revise sentence. An example is provided: The effect of the material parameters on ice arches in a numerical framework that includes both the Maxwell Elasto-Brittle (MEB) including a damage parameterization and the Viscous-Plastic (VP) dynamics.

>> The abstract was completely rewritten.

Following lines after line 2: I assume that this is MEB but it is a little unclear

>> The abstract was rewritten.

Line 20 I think that this should be reformulated. For instance, ice keel don't protect sea-ice from forcing. It creates a friction that resist the forcing. I would reformulate this

>> This was reformulated as suggested by the reviewer, and now reads:

Typically, large landfast ice areas can form and remain stable due to the presence of islands or by the grounding of ice keels on the ocean floor.

Line 35 Ice thickness anomaly is this in time or space? I guess that the influencing factor is the current ice thickness, spatial variation (anomaly).

>> This was referring to ice thickness anomalies from year to year. This sentence was removed in the revised introduction.

Line 47: replace new rheology with new rheologies

>> Corrected as suggested by the reviewer.

Line 67. References to figures in other articles makes it hard to read. Please either add the location on figure 1 or add a map where this can be shown.

>> The locations were added in Figure 1, as suggested by the reviewer.

Line 77 to 82: This part would be well suited for conclusions and/or abstract. The introduction should be more overview of previous studies and an overview of what will be presented. Not results.

>> It is correct that such statements are usually only included in the abstract or conclusions. However, including those at the end of the introduction situates the reader up front and allows him/her to focus on “how we arrived at those conclusions”. It is a style adopted by many authors both in oral presentations and written papers, and recommended in the book by Joshua Schimel “how to write papers that get cited and proposals that gets funded”. We believe it leads to a more active form of presentation that is more engaging for the reader. For this reason, we have opted to leave it in the introduction.

Line 95: Nares Strait has strong tides in the part near Baffin Bay, thus the ocean currents would most likely be an important factor especially before and probably after the fast ice region has formed. Therefore, this should be mentioned in the discussion.

>> As we state in response to the general comments above, the simulations are not sensitive to the source of the forcing, only to the total magnitude. We also rephrase the results so that we refer to the forcing magnitude, rather to the wind speed throughout the revised manuscript. Note also that the regions of high tidal forcing downstream of Nares Strait is rarely landfast (see Hannah et al., 2009, Vincent 2019). This is also clarified at L408-409:

“Note that higher forcing may be frequent in areas associated with strong tides, although these locations correspond to unstable landfast ice areas and recurrent polynyas (Hannah et al., 2009).”

Coriolis is only zero when the ice is not moving.

>> We are mainly concerned with the loading of landfast ice until the break-up and in the derivation of constraints on the mechanical properties of landfast sea ice. It is correct that the subsequent motion after break-up will have small errors (of the order of 10%, Turnbull et al. 2017) given that ice is relatively thin and that the Coriolis term scales with ice thickness. This is clarified on L80-81 of the revised manuscript:

“We assume no grounding on the ocean floor and neglect the Coriolis term. This omission is appropriate for landfast ice, but can result in small errors in drifting ice (Turnbull et al., 2017).”

The discussion of the influence of the ocean is too small.

>> See comment above. The analysis was re-written such that the forcing used on the ice bridge is not exclusively coming from the atmosphere, but can also originate from the ocean. This is clarified at L86-96 in the revised manuscript.

Equation 6 “:” in the equation?. This is described in equation 8. This should be moved here (first place that it is used)

>> Corrected as suggested by the reviewer.

Line 119 lhs and rhs should be written without using a abbreviation.

>> Corrected as suggested by the reviewer.

Line 120- 124. These sentences are a bit hard to follow. Please revise.

>> These sentences were clarified, as suggested by the reviewer. They now read:

The visco-elastic regime of the MEB model (before fracture) is dominated by a fast and reversible elastic response (first term on the left hand side of Eq. 7), with a slow viscous dissipation acting over longer timescales (second term on the left hand side). The reversibility of the elastic deformations implies that the elastic strains return to zero if all loads are removed. This results from a memory of the previous elastic stress and strain states given by the time-derivative in Eq. 7. The Maxwell viscosity term, although orders of magnitude lower than the other terms in the visco-elastic regime, leads to a slow viscous dissipation of this elastic stress memory over long timescales determined by λ (days in our case).

Line 265 Figure 3 No need to show a ARAKAWA grid. This is a standard. I would remove the figure.

>> This figure is removed, as suggested by the reviewer.

Line 317 Remove “-“ 2 times

>> Corrected as suggested by the reviewer.

Line 404 In short the physical solution did not converge until the tolerance is lower than 10^{-10} . How many iterations are required? Is this important for the computational time (how important?).

>> The errors are not due to a difficulty in solving the equations, but rather to the fact that the residual errors are accumulating in the memory terms (instability). The MEB rheology actually converges rapidly, especially given the small time step required by the CFL criterion. The convergence is most time reached within 6-8 outer-loop iterations (fgmres converges in only 1 iteration, given the very small changes in the solution in 0.5s.). This is clarified at L488-493 in the revised manuscript.

Also, using a very low residual tolerance does not solve the problem. This is now better illustrated in Fig. 15 in the revised manuscript. Note that the small timestep, however, is a burden in terms of total time of integration, especially if longer-term simulations are needed. Using a low tolerance increases that burden. For example, on a standard computer (Quad Core Intel Xeon E5-1630 v3, L2 cache of 10.0 MiB with a RAM of 62.63 GiB), the 10h simulations are completed in 4h30 when using a tolerance of 10^{-10} , 2h30 when using a tolerance of 10^{-4} , and 1h30 when using the VP model and a time step of 10min, a tolerance of 10^{-3} and a maximum of 500 outer loop iterations.

Line 447 Nature is a bit more complex than just wind. Orography ocean currents etc. also play a role, thus values like the cohesion of sea ice should be smaller than 21KN/m seems to be a very rough estimate based on parts of the momentum equation. Admitted wind is normally the dominant factor along with the resistance (internal strength)

>> As stated in general comments above, we agree with the reviewer that the tides and thermal stresses are important in the landfast ice break up process. In our ideal simulations, we consider our forcing to be representative of the combined surface forces on the ice, which vary depending on the location. This was clarified at L86-96 and throughout the analysis. The forcing used to derive our cohesion estimates (0.15 N/m^2) is consistent with a typical forcing on landfast ice (10m/s winds or 0.15m/s current). This is now clarified at L402-403. We also changed the wording throughout the text to discuss the

simulation in terms of surface stresses rather than wind magnitude.

Line 473 How does this compare with results from other MEB implementations.

>> To our knowledge, there are only 2 other implementations of the MEB model: The model of Dansereau et al., (2016, 2017) and NeXtSIM (Rampal et al., 2016, 2019). The angles of fracture and type of deformation associated with the damage have not been investigated in details in those studies, but was recently investigated in Dansereau et al. 2019, who demonstrated that the orientation of the lines of fracture does not follow those predicted by the Mohr Coulomb theory. Our findings are consistent to this assessment. These clarifications are included in section 4 in the revised manuscript.

Line 520: is the “:” suppose to be there?

>> Removed, as suggested.

Line 528: It would be very interesting to include this in a VP/EVP model.

>> We agree. This is something that we are currently working on.

Figure 5 text. Top panel? I can only see one panel in figure 5.

>> Corrected as suggested by the reviewer.

Figure 6. This figure should be labeled a through d instead of a1 2 3 b

>> The numbers are referring to the points in Fig 5, which correspond to the damage fields. The figure label was clarified.

Figure 7 Same as 7, Which points?

>> This error in the label is corrected as suggested by the reviewer.

Figure 8: I would say colored dashed lines

>> This error in the label is corrected as suggested by the reviewer.

Figure 10 Dots are very hard to see. It would be nice to increase the size of these.

>> This figure was removed.

Figure 11: Which colored lines? They are defined in figure 8. Are they the same?

>> Removed, as suggested by the reviewer. There are no colored lines.

Figure 12: I would still label these a, b,c and d. Then add to the text.

>> This figure was removed.

Figure 13 which colored lines? Are they the same?

>> [This label error is corrected as suggested by the reviewer.](#)

Figure 14. Please use a,b,c: : References to the residual tolerance are not very easy. Left 10^{-6} and right 10^{-10} does not make sense.

>> [Corrected, as suggested by the reviewer.](#)

Figure 17 Arrows are very hard to see.

>> [Corrected, as suggested by the reviewer.](#)

Figures in general should be in order of them being mentioned in the text. For instance the result section seem to jump back and forth. I assume that when done with the review process they need to be inserted at appropriated places.

>> [As state above, there was a duplicate figure in the manuscript. Removing this figure has resolved this issue. We also removed Figure 10 from the submitted manuscript, which ease the figure flow.](#)

Dansereau, V., Weiss, J., Saramito, P., Lattes, P., and Coche, E.: A Maxwell-Elasto-Brittle rheology for sea ice modeling, *Mercator Ocean Quarterly Newsletter*, pp. 35–40, 2015.

Dansereau, V., Weiss, J., Saramito, P., and Lattes, P.: A Maxwell elasto-brittle rheology for sea ice modelling, *The Cryosphere*, 10, 1339–1359, <https://doi.org/10.5194/tc-10-1339-2016>, 2016.

Hannah, C.G., Dupont, F., Dunphy, M., 2008b. Polynyas and tidal currents in the Canadian arctic archipelago. *Arctic* 62, 83–95

Rampal, P., Bouillon, S., Ólason, E., and Morlighem, M.: neXtSIM: a new Lagrangian sea ice model, *The Cryosphere Discussions*, 9, 735 5885–5941, <https://doi.org/10.5194/tcd-9-5885-2015>, <http://www.the-cryosphere-discuss.net/9/5885/2015/>, 2015.

Rampal, P., Dansereau, V., Olason, E., Bouillon, S., Williams, T., and Samaké, A.: On the multi-fractal scaling properties of sea ice deformation, *The Cryosphere Discussions*, 2019, 1–45, <https://doi.org/10.5194/tc-2018-290>, <https://www.the-cryosphere-discuss.net/tc-2018-290/>, 2019.

Turnbull, I. D., Torbati, R. Z., and Taylor, R. S. (2017), Relative influences of the metocean forcings on the drifting ice pack and estimation of internal ice stress gradients in the Labrador Sea, *J. Geophys. Res. Oceans*, 122, 5970– 5997, doi:10.1002/2017JC012805.

Vincent, R.F. A Study of the North Water Polynya Ice Arch using Four Decades of Satellite Data. *Sci Rep* 9, 20278 (2019). <https://doi.org/10.1038/s41598-019-56780-6>

Answers to tc-2019-210 RC2

March 28th, 2020

Note :

- The referee comments are shown in black,
- The authors answers are shown in blue,
- *Quoted texts from the revised manuscript are shown in italic and in dark blue.*

This manuscript presents an implementation of the recently developed Maxwell Elasto-Brittle rheology for sea ice mechanics within a finite-difference scheme, and the realization of idealized simulations of ice deformation and motion within a channel. This work is quite similar with what was done in [1], however with several differences:

- A finite-difference, instead of a finite-element, numerical scheme is used - the numerical implementation of the MEB rheology is performed exploiting the code framework of a standard VP code.
- the initial condition is a purely homogeneous ice plate (constant thickness, constant elastic and strength properties), without any sort of initial disorder implemented

The effects of material properties and model parameters are then analyzed from a sensitivity analysis using strictly symmetric boundary conditions and geometry.

Overall, this manuscript is clearly written. Most of the results are consistent with [1], proving the robustness of the MEB rheology to adequately simulate sea ice damage, fracture, or strain localization. I am therefore rather favorable to a publication in The Cryosphere. There are however several mistakes, misunderstandings, or points to discuss more thoroughly (e.g., the flow rule and its relationship to the angle of fractures), which should be fixed before final acceptance. They are listed below:

We thank the referees, Dr. Weiss and Dr. Dansereau, for their thorough review of the manuscript and constructive comments.

1) Title: “The material properties of ice bridges...”. This is strange, and unclear: bridges do not have “material properties”. Maybe the authors wanted do say: “The effect of material properties on the simulation of ice bridges in the ..” ?

>> We agree. The title was rephrased as:

“Landfast sea-ice material properties derived from ice bridge simulations using the Maxwell Elasto-Brittle rheology”

2) p3, L65-73, as well as p14, L390-395: The authors argue at different places about the position of the ice bridges, up- or down-wind the channels. This argumentation is not very clear:

- to what extent the situation shown on fig. 1b is systematic ? To the best of my knowledge, ice bridges can take place at different positions along channels (as actually shown on fig. 1b), including along Nares strait (see e.g. fig. 1 of [1]), and I do not know a systematic, statistical analysis of that (but would be happy to learn about such analysis, if any).

>> On L46-53 (in the revised manuscript), we refer to the fact that ice bridges simulated by the MEB model are mostly located downstream of narrow channels, rather than upstream (i.e. as seen in Figs 4,5,7 and 9 in Dansereau et al. 2017). We do not refer to a single specific location. In the Nares strait, the (stable) ice arch does have preferred locations. Fig. 1 from Dansereau et al., 2017 shows some of these positions, usually either in the Lincoln sea (Fig. 1a and b) or in Kane basin (Fig. 1c). These positions can be seen in several landfast ice cover assessments (see for instance Tivy et al 2011, Galley et al. 2012, Yu et al 2013), and are also recently fully described in Vincent (2019).

- in [1], ice breakup occurs in several successive steps, at different locations along the Nares strait. In conclusion, I am not sure that the unique observation of fig 1b can serve as a severe constrain on model parameterizations.

>> We agree with this statement. The break-up of landfast ice is a rapid process during which the temporary ice edges are highly dependent on the pre-existing ice deformations. We cannot reproduce this in our idealized simulation. Here, we rather refer to the formation of stable ice bridges, which are less influenced by these factors. Figure 1 shows such an ice arch in Kane Basin, which remained in place from early March 2018 to mid-June 2018. We have clarified this in the revised manuscript at L46-53, L465-471 and in the figure caption. We also specify that the aim of the paper is the necessary conditions for the simulation of stable ice arches rather than the temporary ice arches formed in the process of landfast ice break-up. In Dansereau et al. 2017, the location of the stable ice arch (i.e. in Figs 4,5,7 and 9) are located downstream of the narrow channels, seldom seen in the Nares Strait (see Vincent 2019).

3) L92-93. Indeed, at the timescales involved in classical climate models (time step of several hours, as in the papers cited), the advection term can be neglected. This might not be true when considering a much smaller model time step (\sim s). What is the time step of the present simulations? Have you done a proper scale analysis taking that time step into account?

>> The time step used in all simulations is 0.5s (now specified at L184 of the revised manuscript and corrected in Table 2). In such a small time scale, the advection term is many orders of magnitude lower than the inertial term (the inertial term scales as $1/T$, T being the time scale). The advection term can however become important at small length scales. In drift ice, it scales as $\rho_i h_i U^2 / L \approx 10^{-3} \text{ N/m}^2$, where ρ_i ($\sim 900 \text{ kg/m}^3$) is the ice density, h_i ($\sim 1 \text{ m}$) is the ice thickness, L ($\sim 2\text{-}10 \text{ km}$) is the space resolution, $U \sim 0.1 \text{ m/s}$ is a typical ice velocity. This is three orders of magnitude smaller than a characteristic surface wind or ocean stress. At the edge of an ice arch, where a discontinuity in sea ice drift is present at small scales (2 km in our case), it remains two orders of magnitude smaller than other terms in the momentum equation. This has been clarified in L80-85 of the revised manuscript.

4) In section 2.1, ice thickening through mechanical redistribution when $A=1$ is not considered. Was such redistribution scheme implemented? If not, this would be a problem, as such scheme, even very simple, and coupled to the MEB rheology, was found to generate realistic ITD [1]. This would

therefore likely affect all the discussion about ice ridges throughout the entire manuscript. If such scheme was implemented, please detail.

>> Mechanical redistribution is taken into account in our simple 1-category model (i.e. ice or open water). When $A=1$ and sea ice convergence occurs, the mean ice thickness increase (see continuity Eq. 4 in the manuscript), but since $A=1$ is capped at one, this leads to the actual thickness of ice in a grid cell (h/A) to increase, i.e. ridging. A simple 1-category model does not resolve the ITD per se, unless the variability in ice thickness is resolved (i.e. unless the model is run at $O(1m)$ resolution, at which sea ice no longer behaves as a 2D material.

5) Equation (1): C is not defined here, but much later (eq. (9)). Please modify.

>> Corrected as suggested by reviewer.

6) L125-127: I would not agree and there seems to be a misunderstanding here: the elasto-brittle component of the MEB rheology is, by construction, associated with small (and reversible) deformations, while the Maxwell component deals with large (and irreversible) deformations. This is therefore fundamentally different from the VP model where the plastic regime is associated with irreversible strains but strain-rate independent stresses (while the Maxwell component of the MEB model is indeed strain-rate strengthening and not strain-rate independent). Please justify in physically-sound way or remove that sentence.

>> These lines were re-written to clarify this statement. As the reviewer points out, the small deformations in the EB component are elastic or reversible, and they are not in the VP model. Here we make the observation that during the fracture process, the larger (and partly still elastic) deformations + viscous dissipation associated with the damage are analog to the plastic regime in the VP model. When a fracture is developing, the stress state is kept on the critical yield curve while the strain rates and damage increase, and the Elastic stiffness and viscosity decrease. In the VP model, the non-linear bulk and shear viscous coefficients reduce with increasing strain rates, such that the stress states (the product of the two) remain on the yield curve. Thus, in both models, the stress state is independent of the deformation rates during the fracturing. The two models do differ, as stated by the reviewer, post fracturing as the VP model does not have a memory of past deformations other than via the continuity equation and its impact on the ice thickness and concentration. In the MEB, the post-fracture elastic deformation remains important unless the damage is large ($d > 0.8$), while deformations are viscous in fully developed fractures. The damage corresponds to a material memory of past deformation. The text in section 2.2 was heavily re-written to clarify this physics, at L118-123 and L200-215.

7) L134-137 and L222: At least in the case of (Tabata, 1955) and (Weeks and Assur, 1967), these authors discuss the creep of bulk saline ice, driven by viscoplasticity at the crystal scale. The concept introduced in the MEB rheology is fundamentally different: a linear viscous term is introduced to account for the cataclastic flow of highly damaged ice, and associated stress relaxations.

>> Here we were referring to the dissipative effect of the viscous term in undamaged ice. We agree that this effect is negligible in terms of deformation in the landfast ice (for example, a sustained stress of $50kN/m$ in our model results in a viscous creep deformation of the order of 10^{-5}), but is significant in dissipating the elastic stress memory over a long time scale. This is clarified at L118-123 in the revised manuscript.

8) L153-154: This statement is wrong: plane stresses were considered in Dansereau et al., 2015, 2016,

2017 and any implementation of the MEB rheology. This is indeed the correct assumption for thin plates. Note however that the impact of such assumption (plane stress vs plane strain) has little consequence on the global behavior. Note also that the constitutive equation present in the early newsletter Dansereau et al., 2015 is that of the generic Maxwell model.

>> The paper of Dansereau et al. (2016) have a factor of $1/(1+\nu)(1-2\nu)$ in the stress-strain relationship, indicating that the authors have used the plane-strain assumption. Dansereau et al. (2017) however do use the plane stress assumption, as pointed out by the reviewer. In the revised manuscript, we remove the reference to the plane-strain assumption in Dansereau et al. (2016), for conciseness.

9) Section 2.2.2. The authors propose to close the damage envelope towards large compressive stresses using eq. (11). This is another difference with the initial MEB model [2]. In principle, I would say “Why not?”. However, several questions arise:

- What is the physical justification of such closure? At the lab scale, the failure envelope of columnar ice loaded under biaxial stresses is indeed closed towards large biaxial stresses (see e.g. [3]). However, the shape of the closure is significantly different from the one proposed on Fig 2 of this manuscript, and failure under such high confinement occurs through spalling, a failure mechanism that is not observed, to my knowledge, in the field (although out-of-plane failure mechanisms might be related). In addition, internal sea ice stresses recorded in the field never reach such strongly confined biaxial stresses, see e.g. [4].

>> See answer below.

Therefore, a second question arises:

- What can be effect of such closure on the model outputs? I would suggest the authors to compare simulations performed with and without this closure to analyze this point. If the effect is limited, as I suspect from above, then the introduction of such weakly-justified closure would represent an unnecessary complication. If some impact is observed on the formation of ice arches and/or ridges, such sensitivity analysis would be useful to understand its origin.

>> Our concern is not the bi-axial compression state (since, as stated by the reviewer, it is rarely observed) but rather the uni-axial compression which can lead to large compressive stresses – i.e. larger than the mechanical strength of sea ice. This is why we argue for the use of a capping in compressive stress: to limit the uniaxial compression. This is specified at L149 in the revised manuscript. This has the side benefit of improving the numerical stability of the model as discussed in section 4.2 in the revised manuscript. The compression capping does influence the simulation results, as discussed in details in section 3.2.4 of the original manuscript (3.1.2 in the revised manuscript): it can cause uni-axial failure along the upstream coastlines, instead of lines of shear fracture propagating at an angle from the island corners, as in the control run simulation.

10) L180-184, as well as L393. About “the lack of strain hardening in the MEB model leads to non-physical results in convergence with the absence of ridge propagation in the direction parallel to the second principal strain (maximum axial compressive strain).” Here, the authors reference (Richter-Menge et al., 2002) on the subject of strain-hardening observed in sea ice. (Richter-Menge et al., 2002) themselves refer to the parameterization of strain-hardening of Hibler (1979), where the maximum compressive strength of the ice is proportional to its thickness $P = P^*h \cdot \exp(-C(1-A))$. The same proportionality is actually used in the MEB (and EB) rheology. Indeed, instead of writing $E \times d$, $\eta \times d$, $\sigma_c \times d$, for the strength parameters in the constitutive equation, and writing the constitutive and momentum equations in terms of a vertically integrated stress, Dansereau et al., 2017, Bouillon et al.,

2015, Rampal et al., 2016, Rampal et al., 2019, etc. all used stress, instead of the vertically integrated stress, and write the rheology term in the constitutive equation as $\text{div}(h\sigma)$. This discussion about “strain-hardening” should be reconsidered in light of this.

>> This is a good point. The lack of strain hardening in our model is related to the fact that we used the vertically integrated stress definition ($\text{div}(\sigma)$ and not $\text{div}(h*\sigma)$ as in other MEB implementations), so that we keep the same numerical/model platform as our standard VP model. In the original submission, we did not adapt the yield criterion accordingly. We now include the thickness dependency in the cohesion (and compressive strength): i.e. $c = c_0 * h * \exp(-C(1-A))$. This is needed for the set of equation (momentum, stress-strain relation and yield criterion) to be equivalent to the previous MEB model implementations. These clarifications are now added in the model description, in section 2. As expected, using the vertically integrated material parameters does not change the model behavior except for the strain hardening associated to increasing thickness now occurring upstream of the channel, and for a reduced stability of the model (the higher cohesion cause higher compressive stresses and increase the instability issue discussed in the paper). We modified the discussion accordingly, and the comment on strain hardening is removed. We also specify that longer time integration is required for the formation of an ice arch upstream of the channel.

In addition, strain-hardening as the result of damage is not supported by experiments on brittle or quasi-brittle materials. A classical illustration is known as the Kaiser stress-memory effect: If a material is damaged up to a given stress, unloaded, and then reloaded, damage will start again when the previous stress will be reached again (e.g., Heap 2009). In case of sea ice, and particularly in the context of ice/structures interactions, the strengthening of crushed, and then recrystallized, ice has been discussed in the literature (e.g. [5]). This process however involves various mechanisms such as sintering of crushed grains, refreezing, which are not only mechanically driven. Consequently, a change in critical stress when the material fail remains to be observed, proven or disproven in the case of sea ice, at the geophysical scale, before formulating physical parameterizations for it.

>> We agree with the reviewer. The strain hardening in our simulations is because of the h-dependency of the material strength parameters (i.e., a thickening of the ice increases the vertically integrated material strength). It is related to the use of vertically integrated stress, and not to the hardening of the ice material itself. The comment on strain hardening was removed from the analysis.

11) Section 2.2.3, and L224-225 “Note that if λ_0 is sufficiently high, the MEB rheology reduces to the Elasto-Brittle rheology (Bouillon and Rampal, 2015; Rampal et al., 2015).” For the EB rheology, cite [6] rightly instead.

>> Corrected as suggested by the reviewer

12) Section 3.2.2, and L534-539. About the flow rule and Mohr-Coulomb failure criterion: “In the MEB model, the angle of fracture does not follow the theory. We speculate that the deviations are related to the absence of a flow rule linking the deformations to the yield curve and the angle of internal friction.” This is confusing. Fracture occurs in an undamaged or partially damaged material. The material “flows”, or undergoes large deformation, once fractured. Therefore, why is the flow law determining the angle of the fractures that precedes the flow? Please explain the mechanism behind this.

>> Here, we use the term “fracturing” to represent the development of damage: in the MEB model, the development of the fracture is not instantaneous, and damage increases over several time steps as the

deformations progress. As such, the locally increasing deformation influences the surrounding strain orientation. We speculate that this influences the stress concentration associated with the fracture that leads to yielding in neighboring cells (see Dansereau et al., 2019). The ice arch and fracture lines are a result of this propagation of local damage in space. If the orientation of the deformation rate tensor was associated with the yield criterion during this process, we speculate that the lines of fracture would follow the Mohr-Coulomb theory, as observed in other models using a flow rule (see Ringeisen et al., (2019) for instance). In the MEB model, they are not and the fracture line orientation does follow the Mohr-Coulomb theory. This result is consistent with those of Dansereau et al., (2019). We have clarified this in the new discussion section of the revised manuscript, at L472-483.

Second, please note that a flow rule is not required to close the system of equations in the case of the MEB (viscous-elastic-brittle) model.

>> We agree with this comment. The point made here is that the deformations during the development of damage might influence the orientation of the lines of fracture. This is consistent with Dansereau (2019), in which the lines of fractures are found to be determined by the stress concentration and the collective spreading of the damage along lines of damage instability.

Note also that the statements from lines 79-81 and 192 are contradictory (“We also show that the simple stress correction used in the damage parameterization corresponds to a flow rule” “This correction does not correspond to a flow rule”).

>> This was indeed not clear. We removed the 1st sentence, and kept the statement at L168-170 in the revised manuscript, i.e. that the stress correction path does not correspond to a flow-rule.

Note also that no flow rule has been determined for sea ice from in-situ observations, while the normal flow rule is not supported by lab-scale observations [4]. “In theory, the angle of internal friction governs the intersection angle between lines of fracture (Marko and Thomson, 1977; Pritchard, 1988; Wang, 2007; Ringeisen et al., 2019)”: Recent and extensive work on the observation and modelling of the failure and localisation of deformation in brittle and granular materials (not just sea ice) have demonstrated that the relationship between the angle of internal friction and the intersection angle between conjugate faults is actually more subtle than predicted by the Anderson’s theory of faulting: e.g., [7-12]. Initially, the Mohr-Coulomb criterion was not implemented in the MEB rheology (and similarly, the internal friction angle not tuned) in order to fit observations of conjugate faults angles in sea ice. It was rather chosen on the basis of stress measurements within sea ice (see [4]) that suggest a reasonably good fit to this criterion (see [2] on that point).

It has been recently shown that, for an elasto-brittle damageable solid, the fault orientation is not given by the Mohr-Coulomb criterion and Anderson’s hypothesis, instead depends on various factors such as the nature of disorder, the Poisson’s ratio, or the confinement [12]. It might be interesting in the future to better constrain the MEB parameterization on this basis, comparing simulation results with large-scale observations of leads/faults within the sea ice cover.

>> Thank you for this comment. We agree that there are many ways other than a normal flow rule to constrain the orientation of deformations. Here, we point out that the damage parameterization should relax the elastic coefficients in a way that leads to a deformation field that is consistent with observations. This would constitute an improvement to the current damage parameterization.

Dansereau, V., Weiss, J., Saramito, P., Lattes, P., and Coche, E.: A Maxwell-Elasto-Brittle rheology for sea ice modeling, *Mercator Ocean Quarterly Newsletter*, pp. 35–40, 2015.

Dansereau, V., Weiss, J., Saramito, P., and Lattes, P.: A Maxwell elasto-brittle rheology for sea ice modelling, *The Cryosphere*, 10, 1339–1359, <https://doi.org/10.5194/tc-10-1339-2016>, 2016.

Dansereau, V., Weiss, J., Saramito, P., Lattes, P., and Coche, E.: Ice bridges and ridges in the Maxwell-EB sea ice rheology, *The Cryosphere*, 11, 2033–2058, 2017.

Galley, R. J., B. G. T. Else, S. E. L. Howell, J. V. Lukovich, and D. G. Barber, 2012: Landfast sea ice conditions in the Canadian Arctic: 1983–2009. *Arctic*, 65, 133–144.

Rampal, P., Bouillon, S., Ólason, E., and Morlighem, M.: neXtSIM: a new Lagrangian sea ice model, *The Cryosphere Discussions*, 9, 735 5885–5941, <https://doi.org/10.5194/tcd-9-5885-2015>, <http://www.the-cryosphere-discuss.net/9/5885/2015/>, 2015.

Rampal, P., Dansereau, V., Olason, E., Bouillon, S., Williams, T., and Samaké, A.: On the multi-fractal scaling properties of sea ice deformation, *The Cryosphere Discussions*, 2019, 1–45, <https://doi.org/10.5194/tc-2018-290>, <https://www.the-cryosphere-discuss.net/tc-2018-290/>, 2019.

Ringeisen, D., Losch, M., Tremblay, L. B., and Hutter, N.: Simulating intersection angles between conjugate faults in sea ice with different viscous–plastic rheologies, *The Cryosphere*, 13, 1167–1186, <https://doi.org/10.5194/tc-13-1167-2019>, <https://www.the-cryosphere.net/13/1167/2019/>, 2019.

Tivy, A., Howell, S. E. L., Alt, B., McCourt, S., Chagnon, R., Crocker, G., Carrieres, T., and Yackel, J. J. (2011), Trends and variability in summer sea ice cover in the Canadian Arctic based on the Canadian Ice Service Digital Archive, 1960–2008 and 1968–2008, *J. Geophys. Res.*, 116, C03007, doi:10.1029/2009JC005855.

Vincent, R.F. A Study of the North Water Polynya Ice Arch using Four Decades of Satellite Data. *Sci Rep* 9, 20278 (2019). <https://doi.org/10.1038/s41598-019-56780-6>

Yu, Y., H. Stern, C. Fowler, F. Fetterer, and J. Maslanik, 2014: Interannual Variability of Arctic Landfast Ice between 1976 and 2007. *J. Climate*, 27, 227–243, <https://doi.org/10.1175/JCLI-D-13-00178.1>

Answers to tc-2019-210 RC3

March 28th, 2020

Note :

- The referee comments are shown in black,
- [The authors answers are shown in blue,](#)
- *Quoted texts from the revised manuscript are shown in italic and in dark blue.*

Review of “The material properties of ice bridges in the Maxwell Elasto-Brittle rheology” by M. Plante, B. Tremblay, M. Losch, and J-F. Lemieux.

The manuscript introduces an implementation of the MEB rheology in the McGill sea ice model and outlines an idealised test-case studied with the model. The paper discusses the experiment results in relation to expected results from theoretical physical grounds, as well as outlining a few sensitivity experiments done on key parameters. The paper is generally well written and understandable. The science is reasonably interesting and good enough to warrant publication in The Cryosphere. I must say though that the paper quite esoteric, caters to a very narrow audience, and has relatively weak conclusions. As with all idealised, large-scale sea-ice experiments, this one suffers from the fact that comparison to theory, as well as the generalisation of the results, is very difficult.

It is interesting to see a new implementation of the MEB rheology, which as far as I know has so far only been implemented by Dansereau et al (2016) and Rampal et al (2019). Also, even though the setup is virtually the same as that of Dansereau et al (2017), the authors of this paper still to point out some interesting characteristics of the MEB rheology, as their approach is sufficiently different from that of Dansereau et al (2017). The main weakness of the paper is that even though there are some interesting points made (e.g. about the lack of strain hardening and the presence of numerical errors), then those are largely lost to other less interesting aspects (e.g. attempts to estimate physical parameters which should be estimated from a realistic setup). Ideally, the authors should reassess what is really interesting and novel here and focus on those aspects.

[We thank the referee for his or her thorough review of the manuscript and constructive comments.](#)

Other general comments:

*) The abstract should be rewritten, as it does not fit well enough the contents of the paper itself.

>> The abstract was re-written to better reflect the manuscript's content, also as per the comment of reviewer #1.

*) The description of the MEB model is much too detailed. It should suffice to briefly describe those parts of the model that are particularly relevant to the experiments conducted here, as well as those points where the current implementation differs from that of Dansereau et al and Rampal et al. The differences should also be justified.

>> We have simplified somewhat the description of the model by eliminating some of the repetitions. The new model description is still more detailed than what the reviewer would like to see however. Sea ice models have been developed mainly by engineers (e.g. Hibler, Flato, Weiss, Sulski); yet they are used by a climate community composed mainly of physicists. While we agree that the model description could be shortened and make reference to previous work, we decided to present a detailed (stand-alone) description of the model, including details that are often trivial to engineers but less so for the climate community. This point is evident when looking at the development of sea ice modeling as used by the climate community in the last 40 years: as of today, most Global Climate Models use a modification of the standard VP model of Hibler published in 1979. Our goal is to make the model physics more accessible to the broader community such that improvement in future GCM relates to model physics (e.g. using the Elastic Anisotropic Plastic (EAP) rheology, the MEB rheology, VP rheology with Mohr-Coulomb and dilatation or the Elastic Cohesive rheology, etc.), not just the numerics.

*) The discussion of the cohesion (3.2.1) should take the following into account: Cohesion scales with the model resolution, so you cannot recommend one cohesion value for all resolutions (Weiss et al., 2007, Schulson et al 2009, Rampal et al 2016)

>> We agree that the cohesion scales with the scale of features as documented in Weiss et al., (2007) and Schulson et al., (2009). Here, we propose a cohesion value that is consistent with ice bridge observations, which are at a scale typical of current sea ice models (10-100km). While Rampal et al., (2016) document the scaling of deformations in the MEB model, it is not clear that the model resolution impacts the cohesion of sea ice. This was tested by repeating the simulation using different spatial resolution, showing no change in the results.

Comparing ice bridges across different straits should take the ice thickness into account. Ice bridges longer than 100 km were probably a regular feature of the Kara Sea fast-ice cover (Divine et al., 2005, Olason, 2016) - although this is changing with a thinning ice cover there.

>> We agree with the reviewer. Note that we now use vertically integrated strength parameters. These changes in ice thickness will influence the ice bridge stability in the model, as it should be.

*) Angle of internal friction (3.2.2): I'm not convinced this is an appropriate setup to discuss the internal angle of friction. I would at least have wanted to see variations in the domain geometry, or better yet a model run with the setup from Ringeisen et al (2019).

>> We agree. Our findings described here raise interesting questions that we are currently working on, using the same numerical set-up as Ringeisen et al, (2019), and will be published in a subsequent paper. This is clarified in the revised manuscript at L480-482:

“This raises the question whether the lines of fracture may be influenced by the stress correction path used in the damage parameterization, which determines the stress state associated to the fractures. These questions are left for future work and will be addressed using a simple uniaxial loading experiment (e.g. Ringeisen et al., 2019).”

*) Conclusions: You have a tendency to restate speculations from the text as demonstrable conclusions in the conclusions section. This is a serious fault which cannot be allowed to stand.

>> The conclusions are now clearly differentiated between demonstrated results, speculated results and future work.

Specific comments:

L45: “minimum viscosity” should be “maximum viscosity”

>> This line was removed in the revised manuscript.

L72: The term “brittle” refers to a certain type of plasticity, so you cannot contrast brittle and plastic (as in “i.e. Brittle [sic] in the MEB, plastic in the EVP”). Sea ice is a brittle plastic, but it can be argued that the (E)VP gives a (too) ductile behaviour to accurately represent sea ice.

>> Brittle is not a type of plasticity, but refers to a mode of fracture with little prior plastic deformation (see Crandall et al., 1978 for a reference book) before fracture. However, we agree that “brittle” should not be used in contrast to plasticity, as brittle materials can undergo plastic deformation after fracture (e.g. glass). This is corrected in the revised manuscript at L51-52:

“These locations differ from the observed ice arch positions in Nares Strait upstream of these channels (e.g., see Fig 1) or in the Lincoln Sea (Vincent, 2019), which are well reproduced by standard VP or EVP models (e.g., Dumont et al., 2008; Rasmussen et al., 2010).”

L75: It should be “an MEB rheology”, not “a MEB rheology”

>> Corrected as suggested by the reviewer.

L75: “implemented in an Eulerian finite difference VP model” - you should elaborate to make this clearer. I didn’t understand what you meant before reading your section 2.3.

>> Clarified as suggested by the reviewer. The revised text now reads:

“we present the implementation of the MEB rheology in our FD numerical framework.”

L122: Strike “, or creep,” as creep usually refers to very slow viscous deformation of the ice (ductile deformation), but the viscous part of the MEB represents the stress relaxation that occurs after a brittle rupture.

>> The viscous term in the MEB model is always present with different relative magnitude, not only post-fracture. While the viscous deformation is very small before the fracture, it is present and slowly dissipates the elastic stress memory, stabilizing the model. This is clarified at L118-123 and L491-492 in the revised manuscript. For example, using the model without the damage parameterization, a

sustained internal stress of 50kN/m induces a viscous creep deformation of order 10^{-5} .

L125: Rewrite the sentence “This brittle component : : :” emphasizing that both models are plastic, but MEB is brittle while VP is ductile.

>> This was rephrased, as suggested by the reviewer. Note however that a brittle material is defined as a material that breaks with little prior elastic deformation and without significant plastic deformation. In the MEB model, the development of the fracture is not instantaneous and the damage increases over several time steps during which the deformations progress but not the stress state. As such, as in the VP model, the development of brittle fractures in the MEB model is parameterized as a plastic deformation. The models differ in the deformation rule (a flow rule is used in the VP model, while the stress-strain relation remains visco-elastic in the MEB) and in the post-fracture deformations. We add these clarifications at L200-215 in the revised manuscript.

Section 2.2.1 seems unnecessary (or at least needlessly long) as it’s a repetition of previous work. Ditto for section 2.2.2, except for the point about the lack of strain hardening, a point I don’t recall being discussed before in the literature. The authors would do well to develop this point further and highlight it in their experiments.

>> We removed self-repetition in this section but did keep some material included in earlier work for the sake of completeness and for the general reader. We also added clarifications on the strain hardening statement, that relates to the use of vertically integrated equations rather than to an actual hardening of the ice material, which is not parameterized in the model.

L207: Replace lowercase nphi with uppercase nPhi (as well as throughout the rest of the text I believe)

>> Corrected as suggested by the reviewer.

L223: Missing unit for nlambda_0

>> The units (s) were added, as suggested by the reviewer.

L224: I don’t think it’s true that for high enough nlambda_0 MEB becomes EB. At any rate, Bouillon and Rampal (2015) and Rampal et al., (2016) are the wrong references for such a statement.

>> The reference has been corrected, as suggested by the reviewer. This can be seen in a simple scale analysis. In the limit where λ_0 tends to infinity, the viscous relaxation term tends to zero, which makes the system of equations reduce to that of the EB model. This is, for example, mostly the case in landfast ice, where $\lambda = \lambda_0 = 10^5$, making the viscous term orders of magnitude smaller than other terms. In damaged ice, however, λ is reduced by 8-9 orders of magnitude such that the viscous term becomes important unless an unrealistically high λ_0 is used.

Section 2.3: After 5 pages of model description we (finally) have something novel. I dare say only the most attentive reader will make it this far, which would be a pity. You should highlight sections 2.3.1 and 2.3.3 and severely shorten everything else in section 2.

>> As we specified above, while we agree that the model description could be shortened and make reference to previous work, we decided to present a detailed (stand-alone) description of the model, including details that are often trivial to engineers but less so for the climate community. Our goal is to make the model physics more accessible to the broader community such that improvement in future

GCM relates to model physics (e.g. EAP, MEB, VP with Mohr-Coulomb and dilatation, Elastic Cohesive, etc.), not just the numerics.

L293: Both Rampal et al. (2016) and Dansereau et al. (2016) use the finite element method for the spatial discretisation. Rampal et al., however, use a Lagrangian advection scheme.

>> This was clarified at L219-221 of the revised manuscript, which now reads:

“... and presents a significant change from previous implementations that use Finite Element methods with a triangular mesh (Rampal et al., 2016, Dansereau et al., 2016) and/or Lagrangian advection scheme (Rampal et al., 2016).”

Section 2.3.3: How does your approach differ from the fixed point iteration used by Dansereau et al. (2016)? As always for numerics the practical implications of performance and accuracy are paramount.

>> The difference is mainly in the IMPLICIT-EXPLICIT treatment of the ice thickness, concentration and damage within the non-linear iterative solver. In Dansereau 2016, the set of equation is solved using (h,A,d) from the previous time-step. Here, we use the IMEX method for these variables, where the explicit equations for (h,A,d) are moved inside the outer loop, such that the solution correspond to a fully implicit solution. This is specified at L290-291 of the revised manuscript:

“This numerical scheme differs from that of Dansereau et al. (2017) who solve the equations using tracers (h, A, d) from the previous time level.”

Section 3: The figures should appear in the order they are referred to in the text.

>> There was a duplicate of one figure in the manuscript that led to confusion in the automatic latex-referencing. We apologize for not noticing this before submission. We have corrected all remaining issues as proposed by the reviewer. Thanks for noticing this.

L356: “This deviation results from the absence of a flow rule in the MEB model” This is a very strong statement, but you never sufficiently show this to be the case.

>> We agree with the reviewer that this is inferred but not demonstrated in the paper. This is the subject of a future paper where we clarify this statement. This is clarified at L482-483. The comments about the flow rule are re-written to better reflect our conclusions at L475-480; the revised text now reads:

“The fact that different angles of internal friction yield the same fracture orientation (...) indicates that the orientation is not directly associated to the yield criterion in the MEB rheology (there is no flow rule in the MEB rheology).”

L369: The statement “[n]ote that unless : : : critical stress” is true, and a key aspect of the MEB model as fracturing increases the damage but does not influence the critical stress. Changing the critical stress would be a completely different approach. You need to justify the “in contrast to real ice features” much, much better for that statement to stand.

>> This was corrected, as suggested by the reviewer. The intuitive weakening of cracked ice is already

simulated by the damage parameter, which increases the effective stress resulting from a given forcing. While it could be argued that the damage could impact the vertically integrated cohesion, it is misleading to state that this coupling between the damage parameter and the critical stress is justified from observations.

L378: I find the use of the word “point” in relation to the figures confusing. Can you use “panel” instead?

>> Corrected as suggested by the reviewer.

L397: The sentence “A physical solution : : :” cannot be allowed to stand as it is. It implies that the approach of Rampal et al. is unphysical, without stating why this is so. It also implies that the suggested approach is physical, but the support given is meagre in terms of physics. What is more, I see no physical reason to relate the yield curve parameters to ice thickness.

>> Based on this and other reviewers’ comments, we opted to use the vertically integrated yield criterion. This solves the issue discussed here and in the original manuscript, as it was mainly the consequence of using vertically integrated stress but a non-integrated yield criterion. That being said, we are not aware of a physical motivation for the inclusion of the pressure term in the momentum equation as in Rampal et al., 2016. It is also explicitly specified in their paper that this term is used to prevent excessively large ridges, therefore is included for numerical reasons, not for physical reasons.

L402: I found this discussion interesting, but it’s tagged onto a very descriptive part of the paper and unlikely to receive much attention as it stands.

>> We agree with the reviewer. We have now created a new section 4 where we collated the text related to the error analysis.

L536: I would not describe sea ice as being granular here. It can be, but the central pack, which MEB should describe, is not - nor is the unbroken ice cover the fractures are propagating through.

>> Corrected as suggested by the reviewer.

L535: Here you state that the discrepancies between simulated and expected fracture angles are due to the use of a scalar damage parameter. However, in the text itself, you appropriately say that you speculate that this is the case. You should also use this formulation in the conclusions, as you never conclusively show why you don’t get the fracture angles you expect.

>> We agree with the reviewer. This has been rephrased in the revised manuscript.

L544: You never showed that these errors are not detectable in a different configuration.

>> We do not claim to demonstrate it here, but explain that it is not possible to quantify it in non-symmetric simulations. The wording is modified to better reflect this in the conclusions of the revised manuscript.

L547: You don’t show that the use of a damage tensor and a different stress correction scheme would solve the problem.

>> This sentence states this as a “possible solution”. We removed this suggestion and leave it for future work in the revised manuscript.

L558: Recommendations for who? You’ve only shown idealized experiments, so it is very hard to recommend anything to people wanting to run a realistic setup.

>> We have removed the bullet-point recommendations as they are repeating the previous text. However, these conclusions are not only meaningful in our model setup; they directly relate to the damage parameterization itself. For instance, we clearly show a mathematical instability in the damage parameterization equations, which are the basis of the MEB model. There are no reasons to believe that this instability is absent in other implementations, unless some undocumented dissipating factors are used.

L559: Again, in the idealized setup you need this - but what is the impact in other scenarios? You should at least make that distinction clear.

>> This has been rephrased to focus on the need to mitigate the instabilities rather than giving a specific tolerance criterion. As stated above, there is no reason to believe that a mathematical instability would not be present in other simulations, unless a different stress correction scheme is used.

L562: You never show this to be the case, it, therefore, doesn’t belong to the conclusions, and certainly not to your recommendations.

>> As stated in earlier comments, we are now using the vertically integrated cohesion in our model. This recommendation is now removed, and the vertically integrated cohesion is now part of the parameterization and should have been present in the first place.

Crandall, S. H., N. C. Dahl and T. J. Lardner, eds., An Introduction to the Mechanics of Solids, 2nd ed., McGraw-Hill, New York, 1978.

Dansereau, V., Weiss, J., Saramito, P., Lattes, P., and Coche, E.: A Maxwell-Elasto-Brittle rheology for sea ice modeling, Mercator Ocean Quarterly Newsletter, pp. 35–40, 2015.

Dansereau, V., Weiss, J., Saramito, P., and Lattes, P.: A Maxwell elasto-brittle rheology for sea ice modelling, The Cryosphere, 10, 1339–1359, <https://doi.org/10.5194/tc-10-1339-2016>, 2016.

Dansereau, V., Weiss, J., Saramito, P., Lattes, P., and Coche, E.: Ice bridges and ridges in the Maxwell-EB sea ice rheology, The Cryosphere, 11, 2033–2058, 2017.

Rampal, P., Bouillon, S., Ólason, E., and Morlighem, M.: neXtSIM: a new Lagrangian sea ice model, The Cryosphere Discussions, 9, 735 5885–5941, <https://doi.org/10.5194/tcd-9-5885-2015>, <http://www.the-cryosphere-discuss.net/9/5885/2015/>, 2015.

Rampal, P., Dansereau, V., Olason, E., Bouillon, S., Williams, T., and Samaké, A.: On the multi-fractal scaling properties of sea ice deformation, The Cryosphere Discussions, 2019, 1–45, <https://doi.org/10.5194/tc-2018-290>, <https://www.the-cryosphere-discuss.net/tc-2018-290/>, 2019.

Ringeisen, D., Losch, M., Tremblay, L. B., and Hutter, N.: Simulating intersection angles between conjugate faults in sea ice with different viscous–plastic rheologies, *The Cryosphere*, 13, 1167–1186, <https://doi.org/10.5194/>

Schulson, E., & Duval, P. (2009). *Creep and Fracture of Ice*. Cambridge: Cambridge University Press. Doi: 10.1017/CBO9780511581397

Weiss, J., Schulson, E. M., and Stern, H. L.: Sea ice rheology from in-situ, satellite and laboratory observations : Fracture and friction, *Earth and Planetary Science Letters*, 255, 1–8, <https://doi.org/10.1016/j.epsl.2006.11.033>, 2007.

The Landfast sea ice material properties of derived from ice bridges in bridge simulations using the Maxwell Elasto-Brittle rheology

Mathieu Plante¹, Bruno Tremblay¹, Martin Losch², and Jean-François Lemieux³

¹Department of Atmospheric and Oceanic Sciences, McGill University, Montréal, Québec, Canada

²Alfred Wegener Institute for Polar and Marine Research, Bremerhaven, Germany

³Recherche en prévision numérique environnementale, Environnement et changement climatique Canada, Dorval, Québec, Canada.

Correspondence: Mathieu Plante (mathieu.plante@mail.mcgill.ca)

Abstract.

The ~~shape and break-up of landfast ice arches in narrow channels depend on the material properties of the sea ice. The effect of the material parameters on ice arches in a sea ice model with the~~ Maxwell Elasto-Brittle (MEB) rheology is investigated. ~~The MEB rheology, which includes a implemented in the Eulerian, Finite Difference (FD) modeling framework commonly used in classical Viscous-Plastic models. The role of the~~ damage parameterization, ~~is implemented using the numerical framework of a Viscous-Plastic model. This configuration allows to study their different physics independently of their numerical implementation. Idealized icebridge simulations~~ the cornerstone of the MEB rheology, in the formation and collapse of ice arches and ice bridges in a narrow channel is investigated. Ice bridge simulations are compared with observations to derive constraints on the mechanical properties of landfast sea ice. Results show that the ~~elastic part of the model together with the damage parameterization allows~~ overall dynamical behavior documented in previous MEB models is reproduced in the FD implementation, such as the localization of the damage in space and time, and the propagation of ice fractures in space at very short time-scales. The fractures orientation is sensitive to the chosen angle of internal friction, but deviates from theory. It is speculated that these deviations stem from the absence of a flow rule in the rheology. Downwind of a channel, the MEB model easily forms ice arches and sustains. ~~In the simulations, an ice arch is easily formed downstream of the channel, sustaining an ice bridge~~ -Using a material cohesion in the range of 15-21 kPa is most consistent with the ice bridges commonly upstream. The ice bridge collapses under a critical surface forcing that depends on the material cohesion. Typical ice arch conditions observed in the Arctic are best simulated using a material cohesion in the range of 5-10 kN m⁻¹. Upstream of the channel, fracture lines along which convergence (ridging) take place are oriented in an angle that depends on the angle of internal friction. Their orientation however deviates from the Mohr-Coulomb theory. The damage parameterization is found to cause instabilities at large compressive stresses, which prevents longer term simulations required for the formation of ice arches is complicated by the absence of a relationship between the ice strength and the ice conditions, and by the presence of numerical errors associated with the damage parameterization. Results suggest that the formation of ice arches upwind of a channel is highly dependent on the rheology and calls for more analysis to determine the necessary conditions for their formation stable ice arches upstream of the channel, between these lines of fracture. Based on these results, we propose that the stress correction scheme used in the damage parameterization be modified to remove numerical instabilities.

1 Introduction

The term landfast ice designates sea ice that is attached to the coastlines, acting as an immobile and seasonal extension of the land. It starts to form in shallow water in the early stages of the Arctic freeze up (Barry et al., 1979; Reimnitz et al., 1978) and grows throughout the Arctic winter, usually reaching its maximum extent in early spring (Yu et al., 2014). Typically, large landfast ice areas ~~are formed when protected from offshore sea ice dynamics, either by~~ can form and remain stable due to the presence of islands or by the grounding of ice keels on the ocean floor (Reimnitz et al., 1978; Mahoney et al., 2007; Selyuzhenok et al., 2017). Where the water is too deep for grounding, landfast ice ~~also forms~~ can also form where ice floes are jammed in narrow passages between islands or pieces of grounded ice. In the Canadian Arctic Archipelago (CAA), this type of ice is referred to as land-locked. The resulting ice bridges, also called ice arches for their characteristic arching edges (Fig. 1), can have a profound influence on sea ice circulation ~~(Melling, 2002; Kwok, 2005)~~ and regional oceanography by the closure of gateways (Melling, 2002; Kwok, 2005), and on regional hydrography by the formation of winter polynyas downstream of the arches (Barber and Massom, 2007; Dumont et al., 2010; Shroyer et al., 2015). Most studies about ~~land-locked ice ice arches~~ focused on the Nares Strait (Fig. 1) and Lincoln Sea ice bridges ~~(Kozo 1991; Moore and McNeil 2018)~~ (Kozo, 1991; Dumont et al., 2008; Dansereau et al., 2018) which affect the export of thick multi-year ice into the Baffin Bay (Kwok and Cunningham, 2010; Ryan and Münchow, 2017). Ice arches however are a seasonal feature in several locations of the Canadian Arctic Archipelago ~~(Marko and Thomson 1977; Sodhi 1997; Divine et al. 2004; Olason 2016)~~ and they play a role in the formation of the extensive landfast ice cover of the Laptev Sea (Selyuzhenok et al., 2015) covers.

Despite decades of observations (Melling, 2002; Kwok, 2005; Moore and McNeil, 2018; Ryan and Münchow, 2017), the formation, persistence and break up of ice arches remain difficult to ~~explain. In particular, ice arches in the Nares Strait (Fig. 1) are largely unpredictable (Melling, 2002; Ryan and Münchow, 2017). A variety of studies suggest that ice arches are influenced by several factors, such as ice thickness anomalies, enhanced northerly winds, tides or the presence of icebergs (Kwok, 2005; Samelson et al., 2006; Moore and McNeil, 2018). If case studies can attribute ice arch formation or break up anomalies to a combination of these factors, other cases with different behaviour can be found under similar conditions (Moore and McNeil, 2018).~~

predict. It is however clear ~~, especially via modeling studies,~~ from modeling studies that the ability of sea ice to form arches relates to the material properties of sea ice. A number of studies showed that ice arches are produced if the rheology includes sufficient material cohesion (Ip, 1993; Hibler et al., 2006; Dumont et al., 2008). Using the ellipse yield curve of Hibler (1979), this can be ~~done achieved~~ either by decreasing the ~~ellipse ratio (Kubat et al., 2006; Dumont et al., 2008)~~ yield curve ellipse aspect ratio (Kubat et al., 2006; Dumont et al., 2008) and/or by extending the ellipse towards larger isotropic tensile strength (Beatty and Holland, 2010; Olason, 2016; Lemieux et al., 2016). The range of parameter values that are appropriate for the production of ice bridges varies between different ~~models~~ numerical studies, suggesting that ~~other model components~~ different

forcing or model implementations may influence the ice arch formation, such as the minimum viscosity (Olason, 2016), ice grounding (Lemieux et al., 2016) and the presence of tides (Lemieux et al., 2018) (Olason, 2016; Lemieux et al., 2016, 2018).

In recent years, new rheology rheologies were proposed to better represent reproduce the observed characteristics of ice failure, such as the preferred orientation of the lines of fracture (Wilchinsky and Feltham, 2004; Schreyer et al., 2006), or the brittle behaviour behavior of sea ice at small scales (Girard et al., 2011; Dansereau et al., 2016). In particular Among this effort, a brittle damage parameterization (Amitrano et al., 1999) was implemented for sea ice modelling in the neXtSIM model (?). The damage parameterization is based on the notion of progressive damage, originally developed in rock mechanic models to reproduce the non-linear (brittle) behaviour in rock deformation and seismicity (Cowie et al., 1993; Tang, 1997; Amitrano and Helmstetter, 2007). In these models, the material damage associated with micro-cracking is simulated by altering the material properties (e.g. the Young Modulus or the material strength) at the model element scale. If heterogeneity is present in the material, the damage parameterization simulates the self-organisation of the microcracks in a macroscopic line of fracture, as observed in laboratory experiments. It was first used for large scale sea ice modeling by Girard et al. (2011) as the basis for a new (Rampal et al., 2016), constituting the cornerstone of the Elasto-Brittle (EB) rheology, later implemented in the fully Lagrangian dynamic-thermodynamic sea ice model neXtSIM (?). The EB rheology was shown to reproduce the statistical and sealing properties of sea ice deformations (Girard et al., 2011), but was limited by the fact that its linear-elasticity only produces reversible deformations. This problem was addressed in the (Girard et al., 2011, EB) and Maxwell Elasto-Brittle rheology (Dansereau et al., 2016) by including a viscous term in the constitutive relation, dissipating the elastic stresses into permanent deformations in the manner of a Maxwell visco-elastic material (Dansereau et al., 2016, MEB) rheologies. The MEB rheology has been shown to reproduce the statistical characteristics of sea ice deformations, such as intermittency, fracture localization and fractality (Dansereau et al., 2017), and is now used in the most recent version of neXtSIM (Rampal et al., 2019).

Dansereau et al. (2017) used idealised and realistic Nares Strait ice bridge simulations to evaluate characteristics of the was shown to produce ice arches in the Nares Strait region that remain stable for several days, and arch fractures that are part of the landfast ice break up process (Dansereau et al., 2017). The simulated stable ice fracture at the geophysical scale produced by the MEB model. The rheology was shown to produce multiple ice arches in Nares Strait. The ice arches in Dansereau et al. (2017) tended to be located downwind of the channels, at the edge of Dansereau et al. (2017) are located downstream of either Smith Sound or Kane Basin (see their Figure 7). Although ice arches downwind of narrow channels are observed in other parts of the CAA (e.g. in the Lancaster Sound, Fig 1a), this location differs Kennedy channel (see orange curve in Fig 1). These locations differ from the observed ice arch position in the Nares Strait, upwind of constriction points positions in Nares Strait upstream of these channels (e.g., see Fig 1b). This behaviour is also different from the ice arches simulated using the) or in the Lincoln Sea (Vincent, 2019), which are well reproduced by standard VP or EVP models, which are also formed upwind of the constriction points (e.g. Dumont et al. 2008; Rasmussen et al. 2010). Since both the MEB and EVP models have a visco-elastic relationship, this different behavior is probably related either (e.g., Dumont et al., 2008; Rasmussen et al., 2010). Whether this difference in behavior stems from the different physics of MEB and VP rheologies or whether it is just due to the different fracture parameterization (i. e. Brittle in the MEB, plastic in the EVP) or to the different numerical frameworks

(finite element methods in Dansereau et al. 2017, finite difference in Dumont et al. 2008). numerical framework used in both models remains an open question.

95 The EB/MEB models so far have been implemented using Lagrangian advection schemes and/or finite element methods (e.g. Rampal et al. 2016; Dansereau et al. 2017). These numerical features, however, make it difficult to compare the different MEB/EB physics with that of the standard VP or EVP rheologies of the modeling community, as these are usually implemented on Eulerian Finite Difference (FD) numerical frameworks. In this paper, we investigate the role of the damage parameterization and the material strength parameters in the formation of ice arches using a MEB rheology that we implemented in an Eulerian finite difference VP model present our implementation of the MEB rheology on the FD numerical framework of the McGill VP sea ice model (Tremblay and Mysak, 1997; Lemieux et al., 2008, 2014). To our knowledge, it is the first time the MEB rheology is implemented in a finite difference framework, such that the on the numerical platform of a VP model such that its different physics can be assessed independently from the numerical implementation. Using idealised channel simulations, we With this model, we investigate the role of the damage parameterization and the material strength parameters in the formation of ice arches, using an idealized model domain capturing the basic features of real-life geometries where ice arches are observed. We show that the stress concentration damage, and thus memory, is dominant in determining the localisation of the stress concentration and localization of ice fractures. We show also show that the orientation of the failure surface does not follow the theory for Coulombic materials, and that a rheology with a dependency between the ice strength and the ice thickness is needed for realistic ridge building. We also show that the simple stress correction used in the damage parameterization corresponds to a flow rule that is independent of the orientation of the failure surface. The stress correction scheme also amplifies numerical convergence errors by orders of magnitude for large compressive states, introducing numerical artifacts that accumulate in the simulated fields stresses. This prevents a fully symmetric solution in the presence of symmetric forcing and governing equations.

115 This The paper is organised as follows. First In section 2, we present our the implementation of the Maxwell Elasto-Brittle rheology in our Finite Difference framework (section 2). We then present a FD numerical framework. A detailed analysis of the break up of the ice bridge simulated by the MEB rheology (is presented in section 3), along with a sensitivity analysis of the results with respect to the yield and other model parameters. Conclusions are summarized in section 4. material parameters. The MEB model performance in simulating compressive fractures is discussed in section 4, with summarized conclusions in section 5.

120 2 Maxwell Elasto-Brittle Model

2.1 Momentum and continuity equations

The simplified momentum equation for the 2D-2D momentum equation describing the motion of sea ice used in this model is is written as:

$$\rho_i h \frac{\partial \mathbf{u}_i}{\partial t} = \nabla \cdot \underline{\sigma} + \underline{\tau}_a - \underline{\tau}_w \mathcal{I}, \quad (1)$$

125 where ρ_i is the ice density, h is the mean ice thickness, \mathbf{u} ($= u\hat{\mathbf{i}} + v\hat{\mathbf{j}}$) is the ice velocity vector, σ is the vertically integrated internal stress tensor, τ_a ($= \tau_{ax}\hat{\mathbf{i}} + \tau_{ay}\hat{\mathbf{j}}$) and τ ($= \tau_a + \tau_w$) is the air-ice surface stress and τ_w ($= \tau_{wx}\hat{\mathbf{i}} + \tau_{wy}\hat{\mathbf{j}}$) is the ice-ocean stress. The advection of momentum is neglected, being orders of magnitude smaller than the other terms in the momentum balance (Zhang and Hibler, 1997; Hunke and Dukowicz, 1997). The ocean current, and thus the sea surface tilt term, is set to zero and the Coriolis term is ignored, as it is identically zero total external surface forcings from winds and ocean currents. Note that we write the momentum equation in terms of the vertically integrated internal sea ice stresses (i.e., $\nabla \cdot \sigma$) as standard in VP models (e.g., Hibler, 1979; Hunke and Dukowicz, 1997; Wilchinsky and Feltham, 2004), as opposed to the mean internal sea ice stresses (i.e., $\nabla \cdot (h\sigma)$) used in previous implementations of the MEB rheology (Dansereau et al., 2016; Rampal et al., 2016). We assume no grounding of ice on the ocean floor and neglect the Coriolis term. This omission is appropriate for landfast ice. These simplifications are reasonable for landfast ice, but can result in small errors in drifting ice (Turnbull et al., 2017). The advection of momentum (which scales as $\rho_i H [U]^2 / L$, where H , $[U]$ and L are the characteristic ice thickness, velocity, and length scales) is three orders of magnitude smaller than a characteristic air or ocean surface stresses (Zhang and Hibler, 1997; Hunke and Dukowicz, 1997). At the edge of an ice arch where a discontinuity in sea ice drift is present at the grid scale (2 km in our case), it remains two orders of magnitude smaller than other terms in the momentum equation.

The total surface stress is defined in terms of an effective stress (τ_{LFI}) that represents the combined wind and ocean forces acting on the landfast ice, and an additional water drag term that only acts on the drifting ice. That is, using the standard bulk formula (with air and water turning angles set to zero, McPhee, 1979), we have:

$$145 \quad \tau_a = \rho_a C_{da} |\mathbf{u}_a| \mathbf{u}_a + \rho_w C_{dw} |\mathbf{u}_w - \mathbf{u}| (\mathbf{u}_w - \mathbf{u}), \quad (2)$$

$$\approx \rho_a C_{da} |\mathbf{u}_a| \mathbf{u}_a - \rho_w C_{dw} |\mathbf{u}_w| \mathbf{u}_w - \rho_w C_{dw} |\mathbf{u}| \mathbf{u}, \quad (3)$$

$$\approx \tau_w = \tau_{LFI} - \rho_w C_{dw} |\mathbf{u}_w| \mathbf{u}_w, \quad (4)$$

where C_{da} and C_{dw} , ρ_a and ρ_w are the air and water drag coefficients, \mathbf{u}_a is the surface wind and ρ_a and ρ_w densities, C_{da} and C_{dw} are the air and water density drag coefficients (see values in Table 2), and \mathbf{u}_a and \mathbf{u}_w are the surface air and water velocities. Note that the cross terms $\mathbf{u}_w \mathbf{u}$ have been neglected. This equation is therefore exact for landfast ice, the focus of this study, and constitutes an approximation only for ice drifting over an ocean current. Below, we specify τ_{LFI} and give the characteristic wind speed and ocean current equivalent to this forcing for reference.

The continuity equations used for the temporal evolution of the mean ice thickness h (volume per grid cell area) and concentration A are written as:

$$155 \quad \frac{\partial h}{\partial t} + \nabla \cdot (h\mathbf{u}) = S_h, \quad (5)$$

$$\frac{\partial A}{\partial t} + \nabla \cdot (A\mathbf{u}) = S_A, \quad (6)$$

where S_h and S_A are thermodynamic sink and source terms for ice thickness and compactness respectively. For simplicity, S_h and S_A are set to zero in this study.

2.2 Rheology

160 2.2.1 Visco-elastic regime

Following (Dansereau et al., 2016), we consider the ice as a visco-elastic-brittle material ~~behaving like a spring and stiff spring and strong dash-pot in series if the stresses are relatively small (Maxwell part), and breaking when larger stresses are present, after which large deformations are possible. The constitutive equation of the Maxwell Elasto Brittle (MEB) model follows the Maxwell rheological model. The corresponding stress-strain relation is that of a Maxwell visco-elastic material:~~

$$165 \quad \frac{\partial \sigma}{\partial t} + \frac{1}{\lambda} \sigma = EC : \dot{\epsilon}, \quad (7)$$

where ~~E is the Elastic Stiffness defined as the vertically integrated Young Modulus of sea ice,~~ λ is the viscous time relaxation ($\lambda = \frac{\eta}{E}$, η being the ~~viscosity~~ vertically integrated viscosity), E is the vertically integrated Elastic Stiffness, C is the elastic modulus tensor and “:” denotes the double dot product of tensors. ~~In generalized matrix form, the tensors C and $\dot{\epsilon}$ is the strain rate tensor. They are written as:~~

$$170 \quad C = \frac{1}{1-\nu^2} \begin{pmatrix} 1 & \nu & 0 \\ \nu & 1 & 0 \\ 0 & 0 & 1-\nu \end{pmatrix} = \begin{pmatrix} C_1 & C_2 & 0 \\ C_2 & C_1 & 0 \\ 0 & 0 & C_3 \end{pmatrix} \quad (8)$$

$$\begin{pmatrix} \dot{\epsilon}_{11} \\ \dot{\epsilon}_{22} \\ \dot{\epsilon}_{12} \end{pmatrix} = \begin{pmatrix} \frac{\partial u}{\partial x} \\ \frac{\partial v}{\partial y} \\ \frac{1}{2} \left(\frac{\partial u}{\partial y} + \frac{\partial v}{\partial x} \right) \end{pmatrix} \quad (9)$$

where ν ($= 0.33$) is the Poisson ratio. The components of the elastic modulus tensor C are derived using the plane stress approximation (i.e., following the original assumption that the vertical stress components are negligible, see for instance ~~Rice 2010~~). Note that we neglect the advection of stress ~~is neglected in this study in the time derivative of Eq. 7~~ as we focus on ~~the landfast ice. In the linear elastic regime (when the main balance is between the~~

~~The visco-elastic regime of the MEB model (before fracture) is dominated by a fast and reversible elastic response (first term on the lhs and the rhs left hand side of Eq. 7), deformations are relatively small, occur over a small time scale and are reversible. As such, the elastic with a slow viscous dissipation acting over longer time scales (second term on the left hand side). The reversibility of the elastic deformations implies that the elastic strains return to zero if all loads are removed ~~and the model includes a material~~. This results from a memory of the strain history. In the viscous-elastic regime (when all three terms are important), viscous deformations, or creep, relax the elastic stresses over a longer time scale if the forcing is sustained,~~

185 which results in permanent deformations. The brittle regime occurs when the internal stresses reach a material yield criterion. In this case, brittle fractures (or cracks) progressively reduce the elastic stiffness and previous elastic stress and strain states given by the time-derivative in Eq. 7. The Maxwell viscosity term, although orders of magnitude lower than the other terms in the visco-elastic ratio, allowing for larger visco-elastic deformations with the same amount of stress. This brittle component is thus comparable to the plastic regime of the standard VP model of Hibler (1979), with deformations that are relatively large, and stresses that are strain rate independent. regime, leads to a slow viscous dissipation of this elastic stress memory over long timescales determined by λ (days in our case).

190 ~~Note that while~~ While Eq. 7 is similar in form to the stress-strain relationship of the Elastic Viscous Plastic (EVP) model (Hunke, 2001), the elastic component in the EVP model ~~does not represent the true elastic behavior of sea ice. Rather, the elastic term~~ was introduced to improve the ~~model convergence and~~ computational efficiency of the VP model, ~~by~~ allowing for an explicit numerical scheme and ~~simple efficient~~ parallelization (Hunke and Dukowicz, 1997). In fact, in the new implementation of the EVP model (Hunke, 2001), elastic waves are faster than the observed elastic waves unless a time-step of several hours or more is used (Williams et al., 2017). In the the MEB model, the elastic component represents the true elastic behavior of sea ice while the viscous relaxation component is introduced to dissipate the elastic strains into permanent deformations. The use of a viscous component is consistent with the observation of viscous creep (Tabata, 1955; Weeks and Assur, 1967) and viscous relaxation (Tucker and Perovich, 1992; Sukhorukov, 1996; Hata and Tremblay, 2015b) in field experiments (Tucker and Perovich, 1992; Sukhorukov, 1996; Hata and Tremblay, 2015b). The viscous relaxation term is also
200 analogous to the viscous term in the thermal stress models of Lewis (1993) and Hata and Tremblay (2015a).

2.2.2 Damage parameterization

2.2.3 Linear Elasticity

The elastic component of the MEB rheology implies that the internal stresses are related to the strains (units of m/m) rather than to ~~In the MEB model, the brittle fracture is simulated using a damage parameterization, which is based on progressive damage models originally developed in the field of rock mechanics to reproduce the non-linear (brittle) behavior in rock deformation and seismicity (Cowie et al., 1993; Tang, 1997; Amitrano and Helmstetter, 2006). In these models, the strain rates (units of s^{-1}). We first write the stress-strain relationship of a 2-D linear elastic solid, that is, ignoring the viscous and brittle components of the rheology (Rice, 2010; Bouillon and Rampal, 2015)):~~
205

$$\sigma_{ij} = \frac{E\nu}{1-\nu^2} \delta_{ij} \epsilon_{kk} + \frac{E(1-\nu)}{1-\nu^2} \epsilon_{ij},$$

210 where E is material damage associated with microcracking is simulated by altering the material properties (e.g. the Young Modulus or the material strength) at the model element (or local) scale. If heterogeneity is present in the material, the damage parameterization simulates the self-organisation of the Elastic Stiffness of sea ice, $\sigma_{i,j}$ are the vertically integrated stresses acting in the j^{th} direction on a plane perpendicular to the i^{th} direction, $\nu (=0.33)$ is microcracks in a macroscopic line of

fracture, as observed in laboratory experiments. It was first used for large scale sea ice modeling by Girard et al. (2011) and is now implemented in the Lagrangian dynamic-thermodynamic sea ice model neXtSIM (Rampal et al., 2019).

The sea ice deformations associated with the brittle fractures are parameterized by a gradual decrease in the Poisson ratio and δ_{ij} is the Kronecker delta. The linear elastic stress component of Eq. 7 is obtained by taking the time derivative of Eq. (??), assuming negligible variations in elastic stiffness E :-

$$\frac{\partial \sigma}{\partial t} = EC : \dot{\epsilon},$$

where “:” denotes an inner double tensor product and where

$$C = \frac{1}{1-\nu^2} \begin{pmatrix} 1 & \nu & 0 \\ \nu & 1 & 0 \\ 0 & 0 & 1-\nu \end{pmatrix} = \begin{pmatrix} C_1 & C_2 & 0 \\ C_2 & C_1 & 0 \\ 0 & 0 & C_3 \end{pmatrix}$$

and

$$\dot{\epsilon}_{ij} = \frac{1}{2} \left[\frac{\partial u_i}{\partial x_j} + \frac{\partial u_j}{\partial x_i} \right] \quad or \quad \begin{pmatrix} \dot{\epsilon}_{11} \\ \dot{\epsilon}_{22} \\ \dot{\epsilon}_{12} \end{pmatrix} = \begin{pmatrix} \frac{\partial u}{\partial x} \\ \frac{\partial v}{\partial y} \\ \frac{1}{2} \left(\frac{\partial u}{\partial y} + \frac{\partial v}{\partial x} \right) \end{pmatrix}$$

The components of the tensor C are derived using the plane stress approximation, (i. e. following the original assumption that the vertical stress components are negligible, see for instance Rice 2010). This form is also used in Bouillon and Rampal (2015); ?, but differs from Dansereau et al. (2015) who used the components derived from the plane strain approximation, in which case the vertical components of strain are zero but the vertical normal stress component (σ_{33}) is non-zero. This should be avoided, as it implies that the vertical stress is of significant order (Rice, 2010) and determined by and viscosity η at the local scale, and consequently as a local increase in the horizontal normal stress: $\sigma_{33} = \nu(\sigma_{11} + \sigma_{22})$. magnitude of the deformation associated with a given stress state. The local increase in deformations results in the concentration of internal stresses in adjacent grid cells, leading to the propagation of the fractures in space. The decrease in elastic stiffness and viscosity is set by a damage parameter d representing the weakening of the ice upon fracturing (Bouillon and Rampal, 2015) . The damage parameter has a value of 0 for undamaged sea ice and 1 for fully damaged ice.

2.2.3 Brittle fracture parameterization

In this model, the critical stress at which the ice fails is determined. The damage increases when the stress state exceeds a critical stress, defined by the Mohr-Coulomb failure criterion. This yield criterion is based on standard for granular materials and in agreement with laboratory experiments (Schulson et al., 2006) and was found to agree with field observations (Weiss et al., 2007). A criterion is further used on the second principal stress ($\sigma_2 = \sigma_I - \sigma_{II}$). We also investigate the use of a compressive cut-off to limit the compression (uni-axial compression ($\sigma_2 = \sigma_I - \sigma_{II}$), see Fig. 2). The yield function can be written in In

240 terms of the stress ~~invariant~~ invariants σ_I and σ_{II} , this can be written as:

$$F(\sigma) = \begin{cases} \sigma_{II} + \mu\sigma_I - c < 0 & \text{Mohr Coulomb} \\ \sigma_I - \sigma_{II} > \sigma_c h e^{-C(1-A)} & \text{Compression cut-off} \end{cases} \quad (10)$$

where

$$c = c_0 h e^{-a(1-A)}, \quad (11)$$

$$\sigma_c = \sigma_{c0} h e^{-a(1-A)}, \quad (12)$$

245 ~~where~~ σ_I is the isotropic normal stress (~~compression~~ defined as negative in compression), σ_{II} is the maximum shear stress, c is the ~~cohesion~~, ~~$\mu = \sin \phi$~~ vertically-integrated cohesion, μ ($= \sin \phi$) is the coefficient of internal friction of ice, ϕ is the angle of internal friction and ~~σ_c is the~~ σ_c is the vertically-integrated uni-axial compressive strength. The ~~cohesion, angle of internal friction and compressive strength are~~ parameterization of c and σ_c follows the form of the internal sea ice pressure in the standard VP model with the ice concentration parameter a set to 20 (Hibler, 1979) , and the cohesion c_0 and compressive
 250 strength σ_{c0} are the material properties derived from in-situ observations (see Table 1 for values and references) and laboratory experiments (Timco and Weeks, 2010). ~~The model values used in our control run~~ Model parameters used in this and other studies are listed in Table 2 along with a summary of the value used in other studies in Table Tables 2 and 3.

~~The fracture of ice is parameterized as a local decrease in elastic stiffness and consequently as a local increase in the magnitude of the elastic deformation associated with a given stress state. The local increase in deformations in the material results in the concentration of internal stresses in adjacent grid cells, leading to the propagation of the brittle fracture in space. The elastic stiffness is written in function of a damage parameter d representing the weakening of the ice upon fracturing ($0 < d \leq 1$, Bouillon and Rampal 2015), with a dependency on the ice thickness and sea ice concentration inspired by the ice strength parameterization of Hibler (1979) :-~~

$$E = Y h e^{-C(1-A)} (1 - d),$$

260 ~~where Y ($= 1$ GPa) is the Young Modulus of undeformed sea ice. This value is smaller than that used in the neXtSIM model (10 GPa, Bouillon and Rampal 2015) and similar to that of the MEB model (0.8 GPa, Dansereau et al. 2016). The damage parameter d has a value of 0 for undamaged sea ice and 1 for fully damaged ice, and represents the amount of fractures and material degradation present in the ice. Note that the yield parameters (~~following~~ Following Rampal et al. (2016), μ , σ_c) in the MEB model are not a function of the damage parameter (nor of the ice thickness or concentration). The decrease in elastic stiffness
 265 when the ice fails yields larger deformations (and potentially changes in h and A) for the same state of stress, but does not change the critical stress (i.e., the ice strength). This is in contrast with a strain-weakening or strain-hardening material, a property that has been observed in sea ice (Richter-Menge et al., 2002). The lack of strain hardening in the MEB model leads to non-physical results in convergence with the absence of ridge propagation in the direction parallel to the second principal strain (maximum axial compressive strain). This will be discussed in section 3.1.2.~~

270 ~~Following ?~~, the introduction of damage upon failure is proportional to the local stress in excess of the yield criterion. A damage factor Ψ ($0 < \Psi < 1$) is used to ~~keep the stress scale the stress back~~ on the yield curve. It is defined as (see appendix A for the derivation Ψ):

$$\sigma_f = \Psi \sigma' \quad \text{with} \quad \Psi = \min\left(1, \frac{c}{\sigma'_{II} + \mu \sigma'_I}\right) \min\left(1, \frac{c}{\sigma'_{II} + \mu \sigma'_I}, \frac{\sigma_c}{\sigma'_I - \sigma'_{II}}\right), \quad (13)$$

where σ_f is the corrected stress lying on the yield curve and σ' is the prior stress state that exceeds the yield criterion. ~~In the following, prime quantities are used to indicate stress terms that are not corrected by the damage factor Ψ .~~ Note that the stress components are all scaled by the same damage factor, ~~following such that the path of the stress correction in stress invariant space follows~~ a line from the uncorrected stress state to the origin (see Fig. 2). ~~This correction does not corresponds~~ ~~The stress correction path does not correspond~~ to a flow rule: ~~only~~ the magnitude of the excess stress is ~~only~~ used to increase the damage parameter. ~~This~~ ~~It~~ determines the magnitude of the strain associated ~~to~~ ~~with~~ a stress state ~~(and indirectly, the strain rate tensor), but not its orientation. This is different from the normal flow rule of Hibler 1979 (see for instance Bouchat and Tremblay 2017), in which the yield curve surface determines the relative importance of shear and divergence in the deformations., but otherwise does not change the visco-elastic relationship in Eq. 7.~~

280 ~~After each fracture event, the damage parameter is updated such that $(1 - d_f) = \Psi(1 - d')$. That is, the damage factors are accumulated in the damage parameter during the simulation, such that the damage gradually increases with each fracture. As the amount of stress overshoot is time-step dependent, the~~ ~~The~~ temporal evolution of the damage parameter ~~is parameterized as follows~~ a simple relaxation with a damage time scale T_d (Dansereau et al., 2016):

$$\frac{\partial d}{\partial t} = \frac{(1 - \Psi)(1 - d)}{T_d}, \quad (14)$$

where T_d is set to the advective time scale associated with the propagation of elastic waves in undamaged ice (~~i.e., $T_d = \Delta x / c_e$, where Δx is being~~ the spatial resolution of the model and c_e the elastic wave speed). ~~Note that the~~ ~~Consequently,~~ ~~the damage at any given time is a function of all previously accumulated damage. No damage healing process was included in this study as we focus on the break up of ice bridges at small time scales. For the same reason, the advection of damage is neglected. The~~ relaxation time scale ~~($T_d / (\Psi - 1)$)~~ in Eq. (14) ~~($T_d / (\Psi - 1)$)~~ is time-step dependent via its dependency on the damage factor Ψ . ~~That is,~~ a larger time step yields larger stress increments and larger excess stresses at each time-level, decreasing the time scale for the damage relaxation. The sensitivity of the damage parameterization on the model time step ~~lead Dansereau et al. (2016) to argue~~ ~~led Dansereau et al. (2016) to suggest~~ that the model time step ~~should~~ be set to exactly T_d , otherwise the damage could travel faster than the elastic waves. We argue that while this point is true when using a fixed damage reduction parameter (as in Amitrano et al. 1999; Girard et al. 2011), the use of a damage factor ~~ψ~~ ~~Ψ~~ relates the damage parameter to the rate of changes in the stress state, which ~~are~~ ~~is~~ associated with the propagation of elastic waves. The propagation of damage in space is thus bounded by the elastic wave speed, and a smaller time-step ~~should be favored if possible~~ ~~in order to resolve the (0.5 s in this study) should be used to respect the CFL criterion associated to the~~ elastic waves.

300 ~~Note that no damage healing process was included in this study as we focus on the break up of ice bridges at small time scales. For the same reason, the advection of damage is neglected.~~

2.2.3 Maxwell-viscosity

305 ~~The viscosity~~ The Elastic stiffness E and Maxwell viscosity η used to define the viscous time relaxation ($\lambda = \frac{\eta}{E}$) is parameterized to change faster with the damage parameter than the elastic stiffness (Dansereau et al., 2016) :

$$\eta = \eta_0(1 - d)^\alpha$$

~~with~~ are written as a non-linear function of d , with a dependency on the ice thickness and sea ice concentration inspired by the ice strength parameterization of Hibler (1979) :

$$E = Y h e^{-a(1-A)}(1 - d), \quad (15)$$

$$310 \quad \eta = \eta_0 h(1 - d)^\alpha, \quad (16)$$

where Y ($= 1 \text{ GN m}^{-2}$, smaller than in Bouillon and Rampal 2015 and similar to Dansereau et al. 2016, see Table 3) is the Young Modulus of undeformed sea ice, η_0 being is the viscosity of undeformed sea ice and α is an integer set to 4 that determines the smoothness of the transition from linear elastic behavior to viscous behavior. This definition ensures that visco-elastic behavior to the viscous term is negligible in undamaged ice, but important in heavily damaged ice (see Eq. 7, where post-fracture viscous behavior (Dansereau et al., 2016). Note that E and η appears in the denominator). Note that as the damage increases asymptotically to 1, the singularity in Eq. 16 (if $d = 1$) never occurs. are defined as in previous implementations except for the linear dependence in ice thickness required because of the use of vertically integrated stress σ .

The relaxation time constant λ in Eq. 7 can then be written using Eq. 15 and 16 is then written as:

$$\lambda = \frac{\eta}{E} = \frac{\lambda_0(1 - d)^{\alpha-1}}{h e^{-C(1-A)}} \frac{\lambda_0(1 - d)^{\alpha-1}}{e^{-a(1-A)}}, \quad (17)$$

320 where λ_0 ($= \eta_0/Y = 10^5$) ($= \eta_0/Y = 10^5$ s, smaller than in Dansereau et al., 2016, but in agreement with observations, see Table 1) is a parameter that corresponds to the viscous relaxation time scale in undamaged sea ice with 1m mean thickness. The value of about one day falls into the range of observations (see Table 1). Note that if In the limit when λ_0 is sufficiently high, the MEB rheology reduces to the Elasto-Brittle rheology (Bouillon and Rampal, 2015; ?). The set tends to infinity, the MEB rheology tends to the Elasto-Brittle rheology (Girard et al., 2011).

325 Note that when a fracture is developing, the stress state is constantly brought back to the yield curve while the damage and the deformation increase. This is comparable to the plastic regime of the standard VP model of Hibler (1979) : in the VP model, the non-linear bulk and shear viscous coefficients reduce with increasing strain rates, such that the stress state (the product of the two) remains on the yield curve while the deformation increases. However, the plastic deformations in the VP model are defined by a normal flow rule, which also determines the orientation of the strain rate tensor (Bouchat and Tremblay, 2017; Ringeisen et al., 2019).

330 In the MEB model, the large deformation associated to the damage is governed by the visco-elastic relationship of Eq. 7 and the yield curve does not directly determine the orientation of the strain rate tensor. The two models also differ post fracturing: the VP model does not have a memory of past deformations other than via the continuity equation and its impact on the ice

thickness and concentration. In the MEB rheology, the damage corresponds to a material memory of past deformations even if the thickness and concentration remain unchanged.

335 The non-linear relationship of the viscous relaxation time scale on d and A ensures that the viscous term is very small in undamaged ice, and dominant in heavily damaged ice (see Eq. 7, where λ appears in the denominator). In this case, the deformations are large, irreversible and viscous. This is different from the standard VP and EVP models in which there is no change in the constitutive equation before or after the ice fracture. The dependency of λ on the mean-ice-thickness-and concentration ensures that both ice concentration also ensures that the total stress tends toward zero for low mean-thickness or concentration (i.e. in free drift), while-but not in a continuous ($A \sim 1, h > 0$) but heavily damaged ice cover behaves as a viscous material.

2.3 Numerical approaches

In this section, we discuss the numerical This model was coded using an Eulerian, FD, implicit numerical scheme, and is the first implementation of the MEB rheology exploiting the code framework of a model on the same numerical framework as the standard VP model. In this This implementation was motivated by the need for a direct comparison between the VP and the MEB rheologies independently from the different numerical approaches, and presents a significant change from previous implementations that use Finite Element methods with a triangular mesh (Rampal et al., 2016; Dansereau et al., 2016) and/or Lagrangian advection scheme (Rampal et al., 2016). In the standard VP numerical framework, the stress components in the momentum equation do not appear explicitly ; instead in the momentum equation. Instead they are written in terms of the non-linear viscous coefficients and strain-rates. This is done in our implementation of For the MEB model, this is accomplished by treating the stress memory term from the time derivation of Eq. 7 as an additional forcing term. The damage parameterization is therefore the only new module that needs to be implemented to be coded.

2.3.1 Time discretization

The model equations are discretized in time using a semi-implicit backward Euler scheme. The uncorrected stress at time level n can then be written using Eq. 7, as:

$$\sigma'^n = \frac{1}{1 + \Delta t / \lambda^n} [E^n \Delta t C : \dot{\epsilon}^n + \sigma^{n-1}] = \xi^n C : \dot{\epsilon}^n + \gamma^n \sigma^{n-1},$$

$$\begin{aligned} \tilde{\sigma}^n &= \frac{1}{1 + \Delta t / \lambda^n} [E^n \Delta t C : \dot{\epsilon}^n + \sigma^{n-1}] \\ &= \xi^n C : \dot{\epsilon}^n + \gamma^n \sigma^{n-1}, \end{aligned} \tag{18}$$

360 where $n - 1$ is the previous time level and where:

$$\xi^n = \gamma^n E^n \Delta t \quad ; \quad \gamma^n = (1 + \Delta t / \lambda^n)^{-1}. \tag{19}$$

Note that $\underline{\sigma^n - \sigma^m}$ is a function of σ^{n-1} , which we refer to as the stress memory. Equation 18 is then substituted in the stress divergence term of Eq. 1, so that the x and y components of the momentum equation can be expanded as :

$$\rho_i h^n \frac{u^n - u^{n-1}}{\Delta t} = \frac{\partial}{\partial x} (\xi^n C_1 \epsilon_{xx}^n) + \frac{\partial}{\partial x} (\xi^n C_2 \epsilon_{yy}^n) + \frac{\partial}{\partial y} (\xi^n C_3 \epsilon_{xy}^n) + \tau_x^n, \quad (20)$$

$$365 \quad \rho_i h^n \frac{v^n - v^{n-1}}{\Delta t} = \frac{\partial}{\partial y} (\xi^n C_1 \epsilon_{yy}^n) + \frac{\partial}{\partial y} (\xi^n C_2 \epsilon_{xx}^n) + \frac{\partial}{\partial x} (\xi^n C_3 \epsilon_{xy}^n) + \tau_y^n, \quad (21)$$

where C_1 , C_2 , and C_3 are the components of the tensor C (Eq. 8) and where the stress memory terms have been included in the forcing, that is :

$$\tau_x^n = \frac{\partial(\gamma^n \sigma_{xx}^{n-1})}{\partial x} + \frac{\partial(\gamma^n \sigma_{xy}^{n-1})}{\partial y} + \tau_{ax}^n + \tau_{wx}^n, \quad (22)$$

$$\tau_y^n = \frac{\partial(\gamma^n \sigma_{yy}^{n-1})}{\partial y} + \frac{\partial(\gamma^n \sigma_{xy}^{n-1})}{\partial x} + \tau_{ay}^n + \tau_{wy}^n. \quad (23)$$

370 The MEB rheology equations can then be implemented in a VP model by setting the VP bulk and shear viscosity to $\zeta_{VP} = \xi \frac{C_1 + C_2}{2}$ and $\eta_{VP} = \xi C_3$ respectively, setting the pressure term to $P = 0$ and adding the stress memory terms.

The variable $\underline{h^n}$, $\underline{A^n}$ and $\underline{d^n}$ (and thus E^n and λ^n) in Eq. 18 to 21 are discretized explicitly, as:

$$\underline{h^n} = h^{n-1} + \nabla \cdot (\mathbf{v}^n h^{n-1} \Delta t), \underline{A^n} = A^{n-1} + \nabla \cdot (\mathbf{v}^n A^{n-1} \Delta t), \underline{d^n} = d^{n-1} + \frac{d^{n-1} \Delta t}{T_d} (\Psi^n - 1), E^n = E_0 h^n d^n e^{-c(1-A^n)}, \quad (24)$$

$$\underline{\lambda^{n,kn}} = \frac{\lambda_0 (d^n)^{\alpha-1}}{h^n e^{-C(1-A^n)}}, \quad (25)$$

375 where the damage factor is computed from Eq. 13 and Eq. 18. using

$$\underline{h^n} = h^{n-1} + \nabla \cdot (\mathbf{v}^n h^{n-1} \Delta t), \quad (26)$$

$$\underline{A^n} = A^{n-1} + \nabla \cdot (\mathbf{v}^n A^{n-1} \Delta t), \quad (27)$$

$$\underline{d^n} = d^{n-1} + \frac{d^{n-1} \Delta t}{T_d} (\Psi^n - 1), \quad (28)$$

$$\underline{\Psi^n} = \min \left(1, \frac{c^n}{\sigma_{II}^n + \mu \sigma_I^n}, \frac{\sigma_c^n}{\sigma_I^n - \sigma_{II}^n} \right), \quad (29)$$

$$380 \quad \underline{c^n} = c_0 h^n e^{-C(1-A^n)}, \quad (30)$$

$$\underline{\sigma_c^n} = \sigma_{c_0} h^n e^{-C(1-A^n)}, \quad (31)$$

2.3.2 Space discretization

The model equations are discretized in space using a centered finite different scheme on an Arakawa C-grid. In this grid, the diagonal terms of the σ and $\dot{\epsilon}$ tensors are naturally computed at the cell centers and the off-diagonal terms at the grid nodes (see

385 ~~Fig.??).~~ The x-component of the momentum equation are written as :

$$\rho_i h_{i,j}^{n-1} \frac{u_{i,j}^n - u_{i,j}^{n-1}}{\Delta t} = C_1 \frac{(\xi^{n-1} \epsilon_{xx})_{i,j} - (\xi^{n-1} \epsilon_{xx})_{i-1,j}}{\Delta x} + C_2 \frac{(\xi^{n-1} \epsilon_{yy})_{i,j} - (\xi^{n-1} \epsilon_{yy})_{i-1,j}}{\Delta x} + C_3 \frac{(\xi_z^{n-1} \epsilon_{xy})_{i,j+1} - (\xi_z^{n-1} \epsilon_{xy})_{i,j}}{\Delta y} + \tau_{x i,j}^n \quad (32)$$

where :

$$(\epsilon_{xx}^n)_{i,j} = \frac{u_{i+1,j}^n - u_{i,j}^n}{\Delta x}, \quad (33)$$

$$(\epsilon_{yy}^n)_{i,j} = \frac{v_{i,j+1}^n - v_{i,j}^n}{\Delta y}, \quad (34)$$

$$390 \quad (\epsilon_{xy}^n)_{i,j} = \frac{u_{i,j}^n - u_{i,j-1}^n}{2\Delta y} + \frac{v_{i,j}^n - v_{i-1,j}^n}{2\Delta x}, \quad (35)$$

$$\tau_{x i,j}^n = \frac{(\gamma^{n-1} \sigma_{xx}^{n-1})_{i,j} - (\gamma^{n-1} \sigma_{xx}^{n-1})_{i-1,j}}{\Delta x} + \frac{(\gamma_z^{n-1} \sigma_{xy}^{n-1})_{i,j+1} - (\gamma_z^{n-1} \sigma_{xy}^{n-1})_{i,j}}{\Delta y} + \tau_{ax i,j}^n + \tau_{wx i,j}^n. \quad (36)$$

The shear terms in Eq. 32 and 36 (ϵ_{xy} , ξ_z and γ_z) are thus defined at the lower-left grid node rather than at the grid center. ~~This-The~~ staggering of the stress components is unavoidable when using the C-grid, and requires node approximations for the scalar values h , A and d (Losch et al., 2010). This is treated on our Cartesian grid with square cells by approximating the scalar prognostic variables at the nodes (h_z , A_z and d_z) ~~as-using~~ a simple average of the neighbouring cell centres, i.e. :

$$h_z = \bar{h}_{i,j} = \frac{h_{i,j} + h_{i-1,j} + h_{i,j-1} + h_{i-1,j-1}}{4}, \quad (37)$$

and similarly for A_z and d_z . The stress-strain coefficients ξ_z and γ_z are then computed using (h_z , A_z and d_z) in Eq. 15, 17 and 19.

The shear stress at the cell centre must also be approximated when computing the stress invariants in the stress correction scheme (Eq. 13). Averaging the shear stress components from the neighboring nodes (as in Eq. 37 for the scalars) ~~cause-causes~~ a checker board instability ~~to-appear~~ in the solution, because of the staggered shear stress corrections and memories. To avoid this, ~~we approximate the the mean~~ shear stress at the cell center ~~using-a-different-shear-stress-is defined using an average of the neighboring shear stress increments~~ ($\xi_z \epsilon_{xy}^n$), ~~which are integrated in another shear stress~~ memory term, defined at the grid center ~~and only used in the damage parameterization, and only average the shear stress increments~~. That is:

$$405 \quad \sigma'_{xy i,j}|_C = \overline{(\xi_z \epsilon_{xy}^n)}_{i,j} + \gamma^{n-1} \sigma_{xy i,j}|_C, \quad (38)$$

where $\sigma'_{xy i,j}|_C$ is the uncorrected shear stress at the grid center, $\overline{(\xi_z \epsilon_{xy}^n)}_{i,j}$ is the shear stress increment averaged as in Eq. 37 and $\sigma_{xy i,j}|_C$ is the corrected shear stress at the grid center from the previous time step. ~~This approximation is only used to calculate the damage factor ψ .~~

Note that the ~~averages in Eq~~ approximations in Eqs. 37 and 38 ~~cause a smoothing of the variables used to define the shear stress state. This may yield significant differences with the previous implementation of the damage parameterization, which was developed for models using a Lagrangian (?) or Finite Element Method (Dansereau et al., 2016) schemes, but~~

would allow insightful comparisons with VP and EVP model simulations using similar discretization schemes are required due to the use of a FD scheme, a notable difference with the other MEB implementations using Finite Element Methods (Dansereau et al., 2016; Rampal et al., 2019).

415 2.3.3 Numerical solution

The discretized equations described above. With n_x tracer (h, A, d) points in the x-direction and n_y in the y-direction, the spatial discretization on our C-grid leads to a system of $N = (n_y(n_x + 1) + n_x(n_y + 1))$ non-linear equations for the velocity components. By stacking all the u components followed by the v ones, we form the vector \mathbf{u} of size N . The non-linear system of equations (momentum) for \mathbf{u}^n and the other discretized equations (Eqs. 24-31) are solved simultaneously using an IMPLICIT EXPLICIT (IMEX) approach (Lemieux et al., 2014). This process As described in the algorithm below, this procedure is based on a Picard solver (Lemieux et al., 2008) which involves an Outer Loop (OL) iteration. At each OL iteration k , the non-linear system of equations (momentum) is linearized and solved using a preconditioned Flexible General Minimum RESidual method (FGMRES). The latest iterate \mathbf{u}^k is used to solve explicitly the damage and continuity equations until the L2 norm. This iterative process is conducted until the L2-norm of the solution residual falls below a set tolerance of $\epsilon_{res} = 10^{-10} \text{ N /m}^2\text{m}^{-2}$.

425 The uncorrected stresses σ'^n is then scaled by the damage factor Ψ^n and stored as the stress memory σ^n for the following time step. This numerical scheme differs from that of Dansereau et al. (2017) who solve the equations using tracers (h, A, d) from the previous time level.

To summarize, the IMEX stepping scheme can be written as :-

1. Start time level n with initial iterate $\mathbf{u}_0 = \mathbf{u}^0$
- 430 do $k = 1, k_{max}$
 2. Linearize the momentum equation non-linear system of equations by using $\mathbf{u}^{n,k-1}, h^{n,k-1}, A^{n,k-1}$ and $d^{n,k-1}$
 3. Calculate $\mathbf{u}^{k,n}$ by solving Eq. 20 and 21 with GMRES $\mathbf{u}^{n,k}$ by solving the linear system of equations with FGMRES
 4. Calculate $\Psi^{n,k} = f(\sigma'^{n,k})$
 5. Calculate $h^{k,n} = f(h^{n,k-1}, \mathbf{u}^{n,k}), A^{n,k} = f(A^{n,k-1}, \mathbf{u}^{n,k}), d^{n,k} = f(d^{n,k-1}, \mathbf{u}^{n,k}, \Psi^{n,k})$
 - 435 6. Calculate $E^{k,n} = f(d^{n,k}, h^{n,k}, A^{n,k}), \lambda^{n,k} = f(d^{n,k}, h^{n,k}, A^{n,k})$
 7. If the Picard solver converged to a residual $< \epsilon_{res}$, stop.
- enddo
8. Update the stress memory $\sigma^n = \Psi^n \sigma'^n$
- 440 where a simple upstream advection scheme is used for $h^{k,n}$ and $A^{k,n}$ in step 5. Note that steps 4, 5, 6 and 8 are performed for all the grid points.

3 Results

In the following, we present a series of ~~ideal-idealized~~ simulations to document the formation and break-up of ice arches with the MEB rheology, and their sensitivity to the choice of mechanical strength parameters. Results from these simulations and
445 observations are used to constrain the material parameters used in sea ice models. Here, we define an ice arch as the location of the discontinuity in the sea ice ~~velocity-and-velocity~~ (and later in the ice thickness and concentration ~~fields-and-fields~~) and the ice bridge as the landfast ice ~~upwind-upstream~~ of the ice arch.

Our model domain is 800 x 200 km with a spatial resolution of 2 km (Fig. 3). The boundary conditions are periodic on the left and right, closed on the top and open on the bottom. Two islands, separated by a narrow channel 200 km long and
450 60 km wide, are located 300 km away from the top and bottom boundaries. The initial conditions for sea ice are zero ice velocity, uniform 1m ice thickness, 100 % concentration and zero damage. A southward ~~wind-foreing~~ forcing T_{LEI} (see Eq. 4) is imposed on the ice surface, and-ramped up from 0 m/s to 0.625 N m⁻² (corresponding to 20 m /ss⁻¹ winds or 0.33 m s⁻¹ surface currents) in a 10h period, a rate well below the adjustment time scale associated with elastic waves. The solution can therefore be considered as steady state at all time, which allows us to determine the critical ~~wind~~-forcing associated with a
455 fracture event.

3.1 Control run

The break up of landfast ice in our simulation proceeds through a series of fracture events that are highly localized in time (see Fig. 4) and space (see Fig. ~~??-and-??~~5 and 6), separated by periods of elastic stress build up (low brittle failure activity). Two major fracture events are seen in the simulation (stage B and D in Fig. 4). The first corresponds to the failure of ice in tension
460 with the development of an ice arch on the ~~downwind-downstream~~ side of the channel (Fig. ~~??~~-5). This occurs on very short time scales (within minutes), and preconditions the formation of an ice bridge over longer time scales (Fig. 5b), in accord with results from Dansereau et al. (2017). The second event corresponds to the collapse of the landfast ice bridge with the break up of ice within and ~~upwind-upstream~~ of the channel (Fig. ~~??~~-6). As for the downstream ice arch, the lines of fractures are formed on short time scales and precondition the location of ridging on the advection time scale (Fig. 6b). The three remaining
465 periods during which few new brittle fractures occur correspond to an elastic landfast ice regime (stage A), a stable ~~downwind downstream~~ ice arch regime (stage C), and a drift ice regime when ice flows within, downstream and upstream of the channel (stage E).

3.1.1 Elastic regime: stage A

In the first stage of the simulation, elastic stress builds up but remains inside the yield curve in the entire domain such that
470 there is no brittle failure activity (Fig. 4, stage A). The sea ice in the elastic regime behaves as an elastic plate and deformations are linearly related to the internal stresses. The elastic stresses are determined by the orientation of the ~~wind-surface forcing~~ with respect to the coastlines: there are large tensile stresses on the ~~downwind-downstream~~ coastlines, compressive stresses on

the upwind-upstream coastlines and shear stresses on the four corners of the channel (Fig. 7). At the vertical line of symmetry (away from channel openings, Fig. 7, dashed blue line), the simulated stress field is in good agreement with the analytical solutions from a 1D version of the momentum equation, giving us confidence in the numerical implementation of the model (see Appendix B and Figure 8). Upstream and downstream of the channel, both stress invariants are important, reaching a maximum in magnitude at the channel corners and decreasing to a local minimum at the center of the channel. In this configuration, the second principal stress alignment (Fig. 7c) is along the x-direction downwind-downstream of the coastlines (where the ice is in uniaxial-uni-axial tension), and along the y-direction upwind-upstream of the coastlines (where the ice is in uniaxial-uni-axial compression). In the downwind-downstream end of channel, the second principal stress alignment takes an arching shape follows the shape of an arch, transitioning to a vertical alignment towards the upwind-upstream channel entrance.

3.1.1 Downstream ice arch: stage B

The formation of the downstream ice arch (Fig. ??) is initiated at a wind-surface forcing of $\sim 3.5 \text{ m/s}$ 0.02 N m^{-2} . The initial fractures are located at the downwind-downstream corners of the channel where the stress state reaches the critical shear strength for positive (tensile) normal stresses (Fig. ??). The fractures then propagate from these locations and form an arch (Fig. ??, point 3 see Fig. 5a). The progression of the fracture into an ice arch is helped by the concentration of stresses at the channel corners and around the subsequent damage. That is, the damage permanently decreases the elastic stiffness, which leads to locally larger elastic deformations and increases the load in the surrounding areas. This results in, leading to the propagation of the fractures in space through regions where the internal stress state was originally sub-critical. This process occurs on very short time scales (within minutes), and preconditions the formation of an arching flaw polynya over longer time scales (Fig. ??b).

To first order, the arching progression of the fracture from the channel corners follows the second principal stress direction (i.e. a failure in uni-axial tension on the plane perpendicular to the maximum tensile stress, see Fig. 7c). This differs from the expected angle of fracture in a coulombic material, at of $\theta = \pm(\pi/4 - \phi/2)$ from the second principal stress orientation (Ringey et al., 2019). This deviation results from the absence of a flow rule in the MEB model. That is, only the Elastic stiffness is changed by the damage parameter to scale back the uncorrected stress to the critical state. The strain rate tensor associated with the fracture is hence determined by the change in stress state at the end of the non-linear solution, rather than by the yield curve surface (see Fig. ??). The flow rule discrepancy is discussed in more details in section 3.2.2, as reported in Dansereau et al. (2019).

3.1.2 Stable ice arch regime: Stage C

A second period of low brittle fracture activity follows the formation of the ice arch (period C in Fig. 4). In this stage, the ice downwind-downstream of the ice arch is detached from the land boundaries and starts to drift. Upstream of the ice arch, the elastic stresses, except for their increase in magnitude due to higher wind forcing, show little changes from stage A. The non-zero brittle fracture activity in this stage is due to the increased damage in regions of already damaged ice; since the local

505 stress state lies on the yield curve, the increasing wind-forcing constantly increases the stress states beyond the yield criterion, leading to further damage. Note that unless the yield parameters depend explicitly on Upstream of the ice arch, the elastic stresses show little changes from stage A, except for their increase in magnitude due to higher forcing (Fig. 9). As the yield parameters (c , σ_c) are not function of the damage, tensile fracturing does not reduce the critical stress, in contrast to real ice fractures. As such, This results in large tensile and shear stresses persist-persisting along and north of the ice arch after the ice arch is formed (Fig. 7b)-its formation. The formation of a stress-free surface could be created-by-defining-the-cohesion-as-a-function-of-the-ice-thickness-and-/or-damage-obtained-by-modifying-the-formulations-of c and σ_{c0} such that they depend on the damage.

3.1.2 Ice bridge collapse: stage D

The second break-up event (Stage D in Fig. 4) corresponds to the fracture of ice upwind-upstream of the channel and the collapse of the ice bridge between-and-upstream-of-the-islands (Fig. ??). This fracture starts at a wind speed of 5.67 m/s on the upwind. The fractures are initiated at a surface forcing of 0.13 N m^{-2} on the upstream corners of the islands where the internal stress reaches the critical shear strength for negative (compressive) normal stresses (green point in Fig. ??). The propagation of damage from these points-locations is composed of two separate fractures (see Fig. 6a). First, a shear fracture progresses downwind-downstream along the channel walls (Fig. ??, point 5). This results, resulting in the decohesion of the landfast ice in the channel from the channel walls, increasing-the. The decohesion of the ice bridge increases the load on the downstream ice arch and in-on the landfast ice north-upstream of the channel. Second, a shear fracture propagates upwind-upstream from the channel corners at an angle 61.858° from the coastline (Fig. ??, point 6). This. The shear fracture orientation corresponds to an angle $\theta = 28.2^\circ$ $\theta = 32^\circ$ from the second principal stress orientation (Fig. 7c). Again, this angle, which also deviates from the theoretical fracture orientation 22.5° in a granular material with $\phi = 45^\circ$, at 22.5° from the second principal stress orientation (Ringeisen et al., 2019). As for the downwind ice arch, the lines of fractures are formed at short time scales and precondition the location of ridging on the advection time scale (Fig. ??b). (Ringeisen et al., 2019).

3.1.3 Drift and ridge building: stage E

The last stage of the simulation (stage E) corresponds to a regime where most of the ice in the domain is drifting. As in Stage C, the non-zero brittle fracture activity corresponds to further damage being produced in the already damaged ice. Once the lines of fracture are completed, the ice bridge collapses and the ice in the channel starts to drift (stage E). In this stage, landfast ice only remains in two wedges of undeformed ice upwind-upstream from the islands in which high compressive stress remains present (see Fig. ??b10a). The remaining continuous areas of undamaged ice drift downward into the funnel as a solid body with uniform velocity, with ridges building at the fracture lines. Note that the-The ridge building is highly localised, with no further stress build-up elsewhere in the domain. This prevents the formation of an ice arch upwind of the channel seen in observations (e.g. in the Lincoln Sea). This unrealistic behaviour of the model is another consequence of the use of constant strength parameters and yield criterion: instead of increasing the pressure with increasing ice thickness during ridging, the

stress field is in a steady state set by the constant critical stress along the deformation lines (see Fig10). The increasing wind forcing is then only balanced by the inertial term and water drag term, resulting virtually in a free drift mode where the ice velocity (and thus the rate of deformation at the ridging lines) increases with the wind forcing. This causes the ice thickness to increase indefinitely at the ridging location. ? mitigated this model artifact by the inclusion of a pressure term in the momentum equation. A physical solution to this problem is to add a dependency between the yield parameters (ϵ (see Fig. 6b), but slowly expands in the direction perpendicular to the lines of fracture. This follows from the increase in material strength with ice thickness, resulting in larger compressive stresses along the ridge such that the ice fracture occurs in the neighboring thinner ice, σ_c) and the ice thickness. This would allow compressive stress to build up along the sliding line and eventually jam the ice. An ice jam would likely result in the formation of an ice arch upstream of the channel, as suggested by the arching orientation of the second principal stress component in the funnel (Fig. 10e). This is left as future work. in a succession of fracture events that are localised in time (see peaks in stage E, in Fig. 4).

Note that the damage field at the end of the simulations is highly sensitive to the solution residual tolerance ϵ_{res} . With time, unless a very low ϵ_{res} is used, the damage fields are no longer horizontally symmetrical about the center of the channel (Fig. 14). This indicates the presence of artifacts in the model, although the solutions always converged to the set precision. An error propagation analysis shows that these asymmetries are produced by the computation of the damage factor ψ (Eq. 13). Assuming that the model is iterated to convergence such that the uncorrected stress state has a relative error of ϵ , the error on the corrected stress is (see derivation in Appendix C):

$$\epsilon_M = \epsilon \sqrt{1 + R},$$

where

$$R = \frac{\sigma'_{II}{}^2 + \mu^2 \sigma'_I{}^2}{(\sigma'_{II} + \mu \sigma'_I)^2}.$$

If $\sigma'_I > 0$ (tensile stress state), $0 < R < 1$ (triangle inequality) and the error of the memory components (ϵ_M) is of the same order as that of the uncorrected stress state ($\epsilon \leq \epsilon_M \leq \sqrt{2}\epsilon$). If $\sigma'_I < 0$ (compressive stress state), we have $R \geq 1$, and the error on the stress memory can become orders of magnitude larger than that of the uncorrected stress state, and the model accuracy and convergence properties are greatly reduced. These errors are stored in the memory terms, and accumulate at each fracture event. Note that as the elastic stress memory is dissipated over the viscous relaxation time scale, this issue can be improved by decreasing the viscous coefficients η_0 . Another solution would be to use a non-linear yield curve which converges to the Tresca criterion ($\sigma_{II} = \text{const}$) for large compressive stresses (e.g. the yield criterion of Schreyer et al. 2006). We however argue that this issue in the damage parameterization should be treated by bringing the stress back onto the yield curve along a different path (e.g. following a line perpendicular to the curve). A different stress correction path would furthermore allow the application of a flow rule based on granular physics. This would require a damage tensor that would scale the components of the stress tensor independently, as commonly used in continuum damage mechanics. Implementing a damage tensor is left for future work.

3.2 Sensitivity to mechanical strength parameters

570 The Mohr-Coulomb yield criterion defines the shear strength of sea ice as a linear function of the normal stress on the fracture plane. In stress invariant coordinates (σ_I, σ_{II}), this can be written in terms of two material parameters: the cohesion c and the coefficient of internal friction $\mu = \sin \phi$ (Fig. 2). The isotropic tensile strength (i.e. the tip of the yield curve) is then a linear function of the two ($\sigma_t = c/\mu$). In this section, we investigate the influence of these material parameters and of ~~a compression~~
575 ~~of the ice fractures in space both upwind and downwind of the channel.~~ the use of a uni-axial compressive strength criterion on the simulated ice bridge. ~~We place a particular focus on the propagation~~

3.2.1 Cohesion

Changing ~~the cohesion c only~~ the cohesion c_0 (with a fixed internal angle of friction ϕ) moves the entire yield curve along the first stress invariant (σ_I) axis. For example, a higher cohesion increases the isotropic tensile strength $\sigma_t = c/\sin \phi$ $\sigma_{t_0} = c_0/\sin \phi$ and also increases the shear strength uniformly for all normal stress conditions. In the ice bridge simulations, the choice of
580 cohesion influences the critical ~~wind-surface~~ forcing associated with the different stages of the simulations but does not change the series of events described in section 3.1 or the orientation of the ice fractures. This is in agreement with results from Dansereau et al. (2017).

The critical ~~wind-surface~~ forcing associated with the ice bridge break up can be related to the cohesion using the 1D steady state momentum equation (see Appendix B for details). Assuming an infinite channel running in the y-direction, the shear
585 stress along the channel walls (σ_{xy}) is given by:

$$|\sigma_{xy}| = \sigma_{II} = \frac{\tau_a W}{2} \frac{\tau_{LFI} W}{2}, \quad (39)$$

where W is the channel width (see Fig. 3). Using the yield criterion (Eq. 10) with $\sigma_I = 0$ (i.e. $\sigma_{II} = c$), the maximum sustainable ~~wind forcing τ_{ac}~~ surface forcing $\tau_{LFI} c$ can be related to the cohesion as:

$$\tau_{ac} = \frac{2c}{W}. \quad (40)$$

590 In the ~~ice bridge~~ simulations, the critical ~~wind~~ forcing for the ~~break-up of the ice bridge (stage D) complete decohesion of ice bridges (point 5 in Fig. 4 and 6) with different widths~~ follows the simple 1D model ~~, although with lower wind forcing values~~ (Fig. 11). This ~~is expected considering the stress concentration occurring indicates that although the fracture is initiated at a weaker forcing due to the concentration of stress~~ at the channel corners ~~and the contribution of the ice upwind and downwind of the non-infinite channel, which pushes and pull on the ice in the channel such that a smaller critical wind forcing is required~~
595 ~~to break the ice~~, the ice arche sustains the increasing load such that the ice bridge remains stable.

Given that ice bridges and arches with a width of ~ 60 km are frequent in the CAA (e.g. Nares Strait, Lancaster Sound, or Prince Regent Inlet), and that the ~~wind speed regularly exceeds~~ surface stresses regularly exceeds 0.15 N m^{-2} (e.g. corresponding to a wind speed of 10 m/s ($\tau_a > 0.15 \text{ N/m}^2 \text{ s}^{-1}$ or a tidal current of $\sim 0.15 \text{ m s}^{-1}$)), this suggests a lower bound on the cohesion of sea ice of at least ~~15 kN/m~~ 5 kN m^{-1} (see ~~green~~ yellow curve in Fig. 11). Similarly, the

600 fact that the ice bridges are rarely larger than 100 km (some are seen intermittently in the Kara Sea, Divine et al. 2004) ~~suggests~~ indicates that the cohesion of sea ice should be smaller than ~~21 kN/m~~ 10 kN m^{-1} (see red curve in Fig. 11). ~~These values are lower than estimates~~ This range ($5\text{-}10 \text{ kN m}^{-1}$) is lower than records from ice stress buoys measurements (40 kPa , Weiss et al., 2007) ~~which includes many driving forces neglected in our simulations, such as thermal stresses (Hata and Tremblay, 2015b) and, to a lesser extent, tides~~ which measure both thermal and mechanical internal stresses at
605 smaller scales (40 kN m^{-2} , Weiss et al., 2007), but agree with estimates from ice arch observations (Sodhi, 1997). Note that higher forcing may be frequent in areas associated with strong tides, although these locations correspond to unstable landfast ice areas and recurrent polynyas (Hannah et al., 2009). Our estimates therefore provide a meaningful bound to be used in sea ice models. Our values are similar to previous large-scale estimates based on wind forcing alone (Tremblay and Hakakian, 2006) and to values used in the neXtSIM model (see Table 3).

610 3.2.2 Angle of internal friction

The angle of internal friction ϕ , analogous to the static friction between two solids, determines the constant of proportionality ($\mu = \sin \phi$) between the shear strength and the normal stress ($\mu = \sin \phi$, see Eq. 10 and Fig. 2). ~~In the following, we vary the~~ Varying the angle of internal friction ~~while keeping the cohesion constant. This ensures that the shear strength of ice without confinement (at $\sigma_T = 0$) is the same in the different simulations, so that the critical wind forcing associated with the ice bridge~~
615 ~~break-up remains of the same order of magnitude. The variations in the angle of internal friction changes the~~ changes in ~~opposite ways the~~ shear strength of ice under tensile and compressive stresses ~~in opposite ways~~: when increasing the angle of internal friction, the shear strength of ice in tension is reduced while that of ice in compression is increased (and vice versa). This affects the ~~magnitude of the wind~~ critical forcing associated with ~~downwind and upwind ice fractures, without affecting that of the fractures along the channel walls (start of stage D). That is, with a larger~~ the downstream and upstream ice fractures.
620 When decreasing ϕ , the ~~downwind downstream~~ ice arch (stage B) forms ~~for weaker winds but stronger wind forcing under a stronger forcing, and a weaker forcing~~ is required for the development of the upstream lines of fracture ~~and the ice bridge collapse. This shows that while sufficient cohesion is necessary for.~~ As such, while the cohesion determines the stability of the landfast ice in the channel, the collapse of the ice bridge ~~depends on the~~ also requires the uni-axial fracture of ice upstream of the channel, which is sensitive to the angle of internal friction.

625 ~~In theory, the~~ The angle of internal friction ~~governs the intersection angle between lines of fracture (Marko and Thomson, 1977; Pritchard~~ That is, the orientation of the failure surface is determined by the point at which the Mohr circle reaches the yield criterion in the Mohr circle space. This point of failure is aligned at angle $\theta = \pm(\pi/4 - \phi/2)$ also determines the shape of the ice fractures: ~~decreasing ϕ leads to an increase in the curvature of the downstream ice arch and intensifies the departure of the upstream lines of fracture~~ from the ~~first principal stress direction (Ringey et al., 2019). In the MEB model, the angle of fracture does not~~
630 ~~follow the theory y-axis~~ (see Fig. 12b). We speculate that the deviations are related to the absence of a flow rule linking the deformations to the yield curve and the angle of internal friction. Note however that the tendency of the fracture orientation remains consistent with the theory: decreasing the angle of internal friction increases the downwind ice arch curvature and the

angle of the fractures (from ϕ). The simulated orientations of the positive x-direction) upwind of the islands. This suggests that despite the absence of a flow rule, the angle of internal friction determines the direction of crack propagation indirectly by changing the material strength. fracture lines (32° and 45° for $\phi = 20^\circ$ and 45°) differ from the orientations of 35° and 22.5° predicted by the Mohr-Coulomb theory, and do not vary linearly with the internal angle of friction.

Note that for angles of internal friction $> 60^\circ$, the upwind lines of fracture propagate away from the boundaries, and a second ice arch forms upwind of the channel (not shown). This angle of internal friction is unrealistically large: previous estimates of the coefficient of friction from ice in situ observations rather suggest values of $30 - 45^\circ$ (see Table 1). This difference stems from the fact that in the Arctic, the ice arches that are commonly observed upwind of a channel are formed when granular floes jam when forced into a constricting channel in which the ice is not landfast. In our experiments, we rather simulate the propagation of ice fractures through the landfast ice upwind of a channel. It should be possible, however, to form these arches during the drift ice regime after the collapse of the ice bridges. In our simulations, two issues impede this process: the lack of compressive stress build up during ridge building and the flow rule (i.e. the path of the stress correction) which favors ridge building over sliding along the landfast edges, limiting the increase in compression directly upwind of the channel.

3.2.3 Tensile strength

The yield curve modifications discussed above (varying c and ϕ) also change the tensile strength (both uniaxial and isotropic) of ice. The tensile strength determines the magnitude of the critical wind surface forcing necessary for the formation of the downwind downstream ice arch (stage B). The tensile stresses downstream from the islands, the tensile stresses can be approximated using the 1D version of the momentum equation as a function of the fetch distance F_{down} (see Fig. 3) between the downwind coast of the islands and from the islands to the bottom boundary of the domain (derivation in Appendix B):

$$\sigma_{yy} = \tau_{aLFI} F_{down}. \quad (41)$$

This can be written as a function of the material parameters using a simplified Mohr Coulomb criterion (Eq. 10) for the 1D case (Appendix B):

$$\sigma_{II} + \frac{\sin \phi}{3} \mu \sigma_I = \frac{1 + 2 \sin \phi}{3} \frac{1 + 2 \mu}{3} \sigma_{yy} < c, \quad (42)$$

where $\nu = 1/3$ was used. Substituting σ_{yy} from Eq. 41 into Eq. 42, the yield criterion can be written in terms of the wind surface forcing and the material parameters:

$$\tau_{aLFI} < \frac{3c}{F_{down}(2 \sin \phi + 1)} \frac{3c}{F_{down}(2 \mu + 1)}, \quad (43)$$

Using our cohesion estimates ($15 \text{ kPa} < c < 21 \text{ kPa}$) and $5 < \mu < 10$, angles of internal friction in the range of observations (30 and 45°) and a typical surface forcing of 0.15 N m^{-2} this would suggest stable bands of landfast ice of extent $F_{down} \sim 100 \text{ km}$ should be sustainable. This is much larger than those observed similar to observations in

the Arctic, where bands of landfast ice rarely exceed a few tens of kilometers unless anchor points are provided by stamukhi (Mahoney et al., 2014). ~~This discrepancy highlights that neglected processes such as waves and tides are important in shaping the landfast ice cover, and may prevent such landfast extent from occurring.~~

3.2.4 Compressive strength criterion

~~Not used in other MEB implementations (Dansereau et al., 2016, 2017), the compressive cut-off offers a limit on the simulated uni-axial compression, which can reach unrealistically large values and cause numerical instabilities (see section 4).~~ Including a compressive strength criterion ($\sigma_I > \sigma_c$) can modify the ~~upwind-upstream~~ fracture event (stage D) by the development of ~~uni-axial~~ compression fractures along the ~~upwind-upstream~~ coast of the islands. ~~The compression strength only affects the simulation if the compressive stress upwind, if the uni-axial compressive stress upstream of the islands exceeds the compressive strength.~~

~~As for the downwind case, the critical wind stress~~ ice strength typically observed in the field ($\sim 40 \text{ kN m}^{-2}$; see Table 1). ~~The critical surface forcing~~ for the development of a compressive fracture can be approximated using the 1D version of the momentum equation. The maximum normal stress at the ~~upwind-upstream~~ coast of the islands is:

$$\sigma_{yy} = \tau_{aLFI} F_{up}. \quad (44)$$

where F_{up} is the distance between the top boundary of the domain and the ~~upwind-upstream~~ coasts of the islands (see Fig. 3). In the ideal case, the compression strength criterion is:

$$\sigma_I - \sigma_{II} = \frac{(1 + \nu)\sigma_{yy}}{2} > \sigma_c. \quad (45)$$

The compression criterion can thus be written as a function of the ~~wind-surface~~ forcing, as:

$$\tau_{aLFI} > \frac{2\sigma_c}{(1 + \nu)F_{up}}. \quad (46)$$

Whether the ice will fail in shear (Mohr-Coulomb criterion) or in compression can be evaluated by substituting ~~τ_a in~~ ~~τ_{LFI}~~ from Eq. (39) ~~by~~ into Eq. 46, yielding the criterion:

$$\frac{(1 + \nu)F_{up}c}{W} > \sigma_c. \quad (47)$$

If this condition is met, the compression strength criterion does not influence the simulation, and the ~~upwind-upstream~~ shear fracture lines develop as in the control simulation (Fig. 13a). If the left hand side term of Eq. 47 is much smaller than σ_c , compression fracture occurs before the ice bridge break up and a ridge forms along the ~~upwind-upstream~~ coastlines, propagating in the channel entrance while the ice in the channel remains landfast (Fig. 13b). If the terms are of similar order, the decohesion of the ice bridge and the compression fractures are initiated simultaneously ~~;~~, ~~such that the~~ compression fracture occurs along the ~~upwind-upstream~~ coastlines but not in the channel entrance, as the ice ~~both in and upwind~~ starts to drift in and upstream of the channel ~~starts to drift~~ (Fig. 13c).

4 Discussion

695 In the Arctic, ice arches are commonly observed upstream of narrow channels, where granular floes jam when forced into the narrowing passage. This requires the ice not to be landfast in the channel itself (Vincent, 2019), as opposed to the simulations presented above where the ice is initially landfast in the model domain. Contrary to results presented in Dansereau et al. (2017) where the presence of floes is simulated by a random seeding of weaknesses in the initial ice field, unstable ice arches upstream of the channel are not present in our simulations. Instead, our experiment simulates the propagation of ice fractures through the landfast ice upstream of a channel, which are akin to a failure in uni-axial compression (Dansereau et al., 2016; Ringeisen et al., 2019).

700 In theory, the angle of internal friction governs the intersection angle between lines of fracture (Marko and Thomson, 1977; Pritchard, 1998). That is, the lines of fracture are oriented at an angle $\theta(= \pi/2 - \phi/4)$ with the second principal stress direction, where the ratio of shear to normal stress is largest. In our simulations, the angles of fracture, although sensitive to the angle of internal friction, do not follow this theory. The fact that different angles of internal friction yield the same fracture orientation (e.g., for $\phi = 20^\circ$ and $\phi = 30^\circ$, see Fig. 12) indicates that the orientation is not directly associated to the yield criterion in the MEB rheology (there is no flow rule in the MEB rheology). However, the orientation of the lines of fracture do have a sensitivity to the angle of internal friction, which suggests that the deformations are at least indirectly influenced by the yield criterion. This is in accord with previous results showing that the fracture orientation is determined by the concentration of stress along lines damage instability (Dansereau et al., 2019). This raises the question whether the lines of fracture may be influenced by the stress correction path used in the damage parameterization, which determines the stress state associated to the fractures. These questions are left for future work and will be addressed using a simple uniaxial loading numerical experiments (e.g. Ringeisen et al., 2019).

715 We speculate that in a longer simulation, ice would eventually jam between the upstream lines of fracture, resulting in the formation of a stable ice arch upstream of the channel. This is suggested by the orientation of the second principal stress component upstream of the channel (Fig. 10c). Longer term simulations, however, are prevented by the presence of numerical instabilities associated with the current damage parameterization. As the integration progresses, the simulated fields lose their longitudinal symmetry about the center line of the domain. This loss of symmetry occurs more rapidly as the residual norm increases (Fig. 14), and is not due to a difficulty in solving the equations: the non-linear solver converges rapidly, within 6 iterations, given the small time step required by the CFL criterion to resolve the elastic waves. The errors are rather related to the integration of the residual norms in the model memory terms in the constitutive equation. The integrated error is only dissipated over a large number of time-step, such that the error in the solution is orders of magnitude larger than the set residual norm tolerance.

720 An error propagation analysis shows that the instabilities are largely attributed to the stress correction scheme and the computation of the damage factor Ψ (Eq. 13). Assuming that the model is iterated to convergence such that the uncorrected stress state has a relative error ϵ , the error on the corrected stress is (see derivation in Appendix C):

$$\epsilon_M = \epsilon\sqrt{1+R}, \quad (48)$$

725 where

$$R = \frac{\sigma'_{II} + \mu^2 \sigma'_I}{(\sigma'_{II} + \mu \sigma'_I)^2}. \quad (49)$$

If $\sigma'_I > 0$ (tensile stress state), $0 < R < 1$ (triangle inequality) and the error on the memory terms (ϵ_M) is of the same order as that of the uncorrected stress state ($\epsilon \leq \epsilon_M \leq \sqrt{2}\epsilon$). If $\sigma'_I < 0$ (compressive stress state), we have $R > 1$, and the error on the stress memory can become orders of magnitude larger than that of the uncorrected stress state, and the model accuracy and convergence properties are greatly reduced. These errors are stored in the memory terms, and accumulate at each fracture event. Note that as the elastic stress memory is dissipated over the viscous relaxation time scale, and this issue could be mitigated by decreasing the viscous coefficients η_0 . Using a compressive strength cut-off capping also offers a limit to the uni-axial compression and reduces this instability. Another solution could be using a non-linear yield curve which converges to the Tresca criterion ($\sigma_{II} = \text{const}$) for large compressive stresses (e.g. the yield criterion of Schreyer et al. 2006). We however argue that this issue in the damage parameterization should be treated by bringing the stress back onto the yield curve along a different path (e.g. following a line perpendicular to the curve). It might also be possible to use a different stress correction path to constrain the orientation of the lines of fractures to the yield criterion. This will be assessed in future work.

5 Conclusions

The MEB rheology ~~was implemented on~~ is implemented in the Eulerian, ~~Finite-Difference~~ FD numerical framework of the McGill sea ice model. We show that the discretized Maxwell stress-strain relationship can be written in a form that resembles that of the VP model, with an additional memory term. The MEB rheology is then simply implemented by redefining the VP viscous coefficients in terms of the MEB parameters and by adding the damage parameterization in a separate module. To our knowledge, ~~this~~ it is the first time the MEB rheology is implemented ~~on~~ in the same framework of a VP or EVP model. This will allow direct comparison of these models using the same numerical platform in future work.

In ~~idealised~~ idealized ice bridge simulations, we show that the damage parameterization allows the ice fractures in the MEB model to propagate over large distances at short time scales. This process relies on the memory of the past deformations included in the model which ~~cause~~ causes a concentration of stresses close to the preexisting damage. We also show that while the choice of yield curve influences the localisation and orientation of the ice fractures, the angles of fracture propagation differ from those expected ~~in a granular material such as sea ice~~ from the Mohr-Coulomb theory. This is ~~due to the simple stress correction scheme using a scalar damage parameter applied on all stress tensor components, such that the flow rule consistent with results from (Dansereau et al., 2019) showing that the fracture orientation is determined by the stress state independently from the orientation at which the ice fracture is occurring. The angles of the fractures could be more physical by the use of a damage tensor, with a stress correction path derived from a physical flow rule. This is left as a future model development~~ planes of damage instability. Preliminary results suggests that the orientation of the fracture lines are influenced by the stress correction scheme. This will be the subject of future work.

The stress correction scheme in the damage parameterization (~~?~~) (Rampal et al., 2016) is also found to cause a problematic ~~propagation of increase in the~~ numerical errors in the stress memory terms. The ~~magnitude of the error propagation growth of errors~~ depends on the magnitude of the compressive stress associated with the ice failure. These errors accumulate in the memory term at each fracture event, creating numerical artifacts that dominate the solutions over time. We argue
760 that this weakness of the damage parameterization should be treated as a numerical issue. ~~Note that these errors are hardly detectable when using material heterogeneity (Dansereau et al., 2016) or realistic boundaries, in which cases the problem is no longer symmetric~~ In previous MEB implementations, asymmetries are expected due to either the asymmetric coastlines and forcing (Rampal et al., 2016) or to the material heterogeneity used to initialise the model (Dansereau et al., 2016), such that ~~this instability difficult to detect~~. A possible solution to this problem would be to use a non-linear yield curve which converges
765 to the Tresca criterion for large compressive stresses (e.g. the yield criterion of Schreyer et al. 2006). ~~The use of a damage tensor and a~~ It may also be possible to eliminate this numerical noise by using a different stress correction scheme ~~would also solve this problem.~~ that does not follow a path to the origin. This will be assessed in future work.

The simulated break up of the landfast ice bridge occurs with two main fracture events. First, an ice arch develops at the ~~downwind downstream~~ end of the channel, shaping the edge of the ice bridge in the channel. This ice arch forms in all
770 simulations and is stable in shape as long as the ice bridge remains in place, with a curvature that increases for smaller angles of internal friction. Second, shear fractures are formed at the ~~upwind upstream~~ end of the channel, resulting in the decohesion of the channel ice bridge and in the formation of landfast wedges ~~upwind upstream~~ of the islands. ~~The angle of the landfast ice wedges depend on the angle of internal friction.~~ Based on the simulation results, we determined that the parameterized cohesion most consistent to the observed ice bridges in the Arctic are in the range of ~~15-21 kPa, that is in the lower range of~~
775 ~~previous estimate. This result is consistent with the fact that only the wind forcing is considered in these idealized simulations, other forcings such as tides, ocean currents and thermal forces are likely acting in conjunction with the wind forcing.~~ ~~5-10 kN m⁻², lower than stress buoys which measure both dynamical and thermal stresses at smaller scales but in the range of values previously associated to ice arch observations.~~

~~Based on these results, these are our recommendations for using the MEB model:-~~

780 ~~A very low solution residual tolerance $\epsilon_{res} < 10^{-10}$ should be use to limit the accumulation of errors associated to the correction scheme.-~~

~~The cohesion should be limited to $c < 21$ kPa.-~~

~~The cohesion should be written as a function of the ice condition (i. e as E , pr P^* in the VP models). This should prevent the formation of unrealistically large ridges.-~~

785 ~~An alternative stress correction scheme should be developed to limit the accumulation of errors in the stress memory terms.-~~

Code availability. Our sea-ice model code and outputs are available upon request.

Appendix A: Damage factor Ψ

Let σ'_I and σ'_{II} be the stress invariant at time level n before the correction is applied, and σ_{If} and σ_{IIf} the corrected stress invariant lying on the yield curve. Following Bouillon and Rampal (2015) we use a damage factor Ψ ($0 < \Psi < 1$) to reduce the elastic stiffness and bring the stress state onto the yield curve. I.e. :

$$\sigma_{If} = \Psi\sigma'_I \quad ; \quad \sigma_{IIf} = \Psi\sigma'_{II}. \quad (\text{A1})$$

Substituting these relations into the Mohr Coulomb criterion ($\sigma_{IIf} + \mu\sigma_{If} = c$) we solve for Ψ :

$$\Psi = \frac{c}{\sigma'_{II} + \mu\sigma'_I}. \quad (\text{A2})$$

Note that this relation implies that the stress correction is done following a line from the stress state (σ'_I, σ'_{II}) to the origin (see Fig. 2). This scheme stems from the use of a single damage factor applied on the elastic stiffness, which is linear to each of the stress components, i. e., the correction is applied equally to each stress component. applying the damage factor to each individual stress components. Other paths could be used for the correction (e.g. following a vertical or horizontal line), but would require the use of a different stress factor for each component the different components of the stress tensor (i. e. using a damage tensor, rather than a damage parameter). This could be used to cure the error propagation problem when large compressive stresses are present (see Appendix C).

Appendix B: Analytical solutions of the 1D momentum equation

Considering an infinite channel of landfast ice ($u = 0$) along the y -direction with wind forcing $\tau_a = \tau_{ay}$ and water stress $\tau_w = 0$ forcing $\tau_{LFY} = \tau_y$, we write the 1D steady state momentum equation as:

$$\frac{\partial\sigma_{xy}}{\partial x} + \tau_{ayy} = 0, \quad (\text{B1})$$

where we have neglected the $\partial/\partial y$ terms. In this case, the normal stress is zero in the entire channel and the stress invariants are $\sigma_I = 0$, $\sigma_{II} = \sigma_{xy}$. The shear stress at any arbitrary point x across the channel can be determined by integrating Eq. B1 from the channel center ($x = 0$) to x :

$$\sigma_{xy} = -\tau_{ayy}x. \quad (\text{B2})$$

By symmetry, the maximum shear stresses in the channel are located at the channel walls, at $x = \pm \frac{W}{2}$ where W is the width of the channel. The maximum shear stress invariant on the channel walls is then:

$$\sigma_{II} = \frac{W\tau_{ay}}{2} \frac{W\tau_y}{2}. \quad (\text{B3})$$

Similarly, we find the analytical solution for the normal stresses in a band of landfast ice with width L_y along an infinite coastline running in the x direction, with a wind forcing $\tau = \tau_{ay}$ and water drag $\tau_w = 0$ with a surface forcing $\tau_{LEI} = \tau_y$, by

integrating the 1D momentum equation in which the $\partial/\partial x$ terms are neglected. I.e. :

$$815 \quad \frac{\partial \sigma_{yy}}{\partial y} + \tau_{ayy} = 0, \quad (B4)$$

$$\sigma_{yy} = -\tau_{axy}y. \quad (B5)$$

Placing the landfast ice edge (where $\sigma_{yy} = 0$) at $y = 0$, the largest compressive stresses will be located along the coast, at $y = -L_y$. Note that in this case, shear stress is zero in the entire land-fast ice and the stress invariants are function of both σ_{xx} and σ_{yy} :

$$820 \quad \sigma_{yy} = EC_1 \epsilon_{yy}, \quad (B6)$$

$$\sigma_{xx} = EC_2 \epsilon_{yy} = \nu \sigma_{yy}, \quad (B7)$$

$$\sigma_I = \frac{\sigma_{xx} + \sigma_{yy}}{2} = \frac{(1 + \nu)\sigma_{yy}}{2}, \quad (B8)$$

$$\sigma_{II} = \sqrt{\left(\frac{\sigma_{yy} - \sigma_{xx}}{2}\right)^2} = \frac{(1 - \nu)\sigma_{yy}}{2}. \quad (B9)$$

This allows to write the Mohr-Coulomb criterion in terms of σ_{yy} :

$$825 \quad \sigma_{II} + \sin \phi \sigma_I = \frac{1 + 2 \sin \phi}{3} \sigma_{yy} < c, \quad (B10)$$

Appendix C: Error propagation analysis

The error δF associated with a function $F(X, Y, Z, \dots)$ with uncertainties $(\delta x, \delta y, \delta z, \dots)$ is given by:

$$\delta F = \sqrt{\left(\frac{\partial F}{\partial X}\right)^2 \delta x^2 + \left(\frac{\partial F}{\partial Y}\right)^2 \delta y^2 + \left(\frac{\partial F}{\partial Z}\right)^2 \delta z^2 + \dots} \quad (C1)$$

830 In the damage parameterization, the components of the corrected stress tensor used as the memory terms (σ_{ijM}) can be written in terms of the uncorrected stress tensor (σ'_{ij}) and the damage factor Ψ (Eq. 13):

$$\sigma_{ijM} = \Psi \sigma'_{ij}. \quad (C2)$$

Using Eq. A2, this can be rewritten in terms of the uncorrected stress invariants (σ'_I, σ'_{II}):

$$\sigma_{ijM}(\sigma'_{ij}, \sigma'_I, \sigma'_{II}) = \frac{c \sigma'_{ij}}{\sigma'_{II} + \mu \sigma'_I} \quad (C3)$$

835 Assuming that the model has converged to a solution within an error on the stresses $\delta \sigma'_{ij} = \epsilon \sigma'_{ij}$, $\delta \sigma'_I = \epsilon \sigma'_I$, $\delta \sigma'_{II} = \epsilon \sigma'_{II}$, where ϵ is a small number, the model convergence error propagates on the stress memory with an error of :

$$\delta \sigma_{ijM} = \sqrt{\left(\frac{\partial \sigma_{ijM}}{\partial \sigma'_{ij}}\right)^2 \delta \sigma'^2_{ij} + \left(\frac{\partial \sigma_{ijM}}{\partial \sigma'_I}\right)^2 \delta \sigma'^2_I + \left(\frac{\partial \sigma_{ijM}}{\partial \sigma'_{II}}\right)^2 \delta \sigma'^2_{II}}. \quad (C4)$$

Substituting $(\delta\sigma'_{ij}, \delta\sigma'_I, \delta\sigma'_{II})$ for ϵ and using Eq. C3, we obtain:

$$\delta\sigma_{ijM} = \sqrt{\frac{c^2}{(\sigma'_{II} + \mu\sigma'_I)^2} \epsilon^2 \sigma'^2_{ij} + \frac{c^2 \sigma'^2 \mu^2}{(\sigma'_{II} + \mu\sigma'_I)^4} \epsilon^2 \sigma'^2_I + \frac{c^2 \sigma'^2}{(\sigma'_{II} + \mu\sigma'_I)^4} \epsilon^2 \sigma'^2_{II}}, \quad (C5)$$

or:

$$840 \quad \delta\sigma_{ijM} = \epsilon\sigma_{ijM} \sqrt{1 + \frac{\sigma'^2_{II} + \mu^2 \sigma'^2_I}{(\sigma'_{II} + \mu\sigma'_I)^2}}. \quad (C6)$$

Assuming that error on the stress memory components (ϵ_M) has the form $\delta\sigma_{ijM} = \epsilon_M \sigma_{ijM}$, we can express the relative error of the stress memory components as a function of the stress invariants as :

$$\epsilon_M = \epsilon \sqrt{1 + R} \quad (C7)$$

where

$$845 \quad R = \frac{\sigma'^2_{II} + \mu^2 \sigma'^2_I}{(\sigma'_{II} + \mu\sigma'_I)^2} \quad (C8)$$

Author contributions. M. Plante coded the model, ran all the simulations, analyzed results and led the writing of the manuscript. B. Tremblay participated in regular discussions during the course of the work and edited the manuscript. M. Losch participated in regular discussions during M. Plante research stays in Germany and edited the manuscript. J-F. Lemieux participated in the implementation of the MEB rheology and provided edits on the manuscript.

850 *Competing interests.* The authors declare that they have no conflict of interest.

Acknowledgements. Our sea-ice model code and outputs are available upon request. Mathieu Plante would like to thank the Fonds de recherche du Québec – Nature et technologies (FRQNT) for financial support received during the course of this work. Bruno Tremblay is grateful for support from the Natural Science and Engineering and Research Council (NSERC) Discovery Program and the Office of Naval Research (N000141110977). This work is a contribution to the research program of Québec-Océan and of the ArcTrain International
855 Training Program. We acknowledge the use of imagery from the NASA Worldview application (<https://worldview.earthdata.nasa.gov>), part of the NASA Earth Observing System Data and Information System (EOSDIS).

References

- Amitrano, D. and Helmstetter, A.: Brittle creep, damage and time to failure in rocks, *Journal of Geophysical Research : Solid Earth*, 111, B11 201, <https://doi.org/10.1029/2005JB004252>, <https://hal.archives-ouvertes.fr/hal-00172671>, 2006.
- 860 Amitrano, D., Grasso, J.-R., and Hantz, D.: From diffuse to localised damage through elastic interaction, *Geophysical Research Letters*, 26, 2109–2112, 1999.
- Barber, D. and Massom, R.: Chapter 1 The Role of Sea Ice in Arctic and Antarctic Polynyas, in: *Polynyas: Windows to the World*, edited by Smith, W. and Barber, D., vol. 74 of *Elsevier Oceanography Series*, pp. 1 – 54, Elsevier, [https://doi.org/https://doi.org/10.1016/S0422-9894\(06\)74001-6](https://doi.org/https://doi.org/10.1016/S0422-9894(06)74001-6), <http://www.sciencedirect.com/science/article/pii/S0422989406740016>, 2007.
- 865 Barry, R., Moritz, R., and Rogers, J.: The fast ice regimes of the Beaufort and Chukchi Sea coasts, Alaska, *Cold Regions Science and Technology*, 1, 129–152, [https://doi.org/10.1016/0165-232X\(79\)90006-5](https://doi.org/10.1016/0165-232X(79)90006-5), <http://linkinghub.elsevier.com/retrieve/pii/0165232X79900065>, 1979.
- Beatty, C. K. and Holland, D. M.: Modeling Landfast Sea Ice by Adding Tensile Strength, *American Meteorological Society*, 40, 185–198, <https://doi.org/10.1175/2009JPO4105.1>, 2010.
- 870 Bouchat, A. and Tremblay, B.: Using sea-ice deformation fields to constrain the mechanical strength parameters of geophysical sea ice, *Journal of Geophysical Research: Oceans*, 122, 5802–5825, <https://doi.org/10.1002/2017JC013020>, <https://agupubs.onlinelibrary.wiley.com/doi/abs/10.1002/2017JC013020>, 2017.
- Bouillon, S. and Rampal, P.: Presentation of the dynamical core of neXtSIM, a new sea ice model, *Ocean Modelling*, 91, 23–37, <https://doi.org/10.1016/j.ocemod.2015.04.005>, <http://dx.doi.org/10.1016/j.ocemod.2015.04.005>, 2015.
- 875 Cowie, P. A., Vanneste, C., and Sornette, D.: Statistical physics model for the spatiotemporal evolution of faults, *Journal of Geophysical Research: Solid Earth*, 98, 21 809–21 821, <https://doi.org/10.1029/93JB02223>, <https://agupubs.onlinelibrary.wiley.com/doi/abs/10.1029/93JB02223>, 1993.
- Dansereau, V., Weiss, J., Saramito, P., Lattes, P., and Coche, E.: A Maxwell-Elasto-Brittle rheology for sea ice modeling, *Mercator Ocean Quarterly Newsletter*, pp. 35–40, 2015.
- 880 Dansereau, V., Weiss, J., Saramito, P., and Lattes, P.: A Maxwell elasto-brittle rheology for sea ice modelling, *The Cryosphere*, 10, 1339–1359, <https://doi.org/10.5194/tc-10-1339-2016>, 2016.
- Dansereau, V., Weiss, J., Saramito, P., Lattes, P., and Coche, E.: Ice bridges and ridges in the Maxwell-EB sea ice rheology, *The Cryosphere*, 11, 2033–2058, 2017.

- Dansereau, V., Démary, V., Berthier, E., Weiss, J., and Ponson, L.: Collective Damage Growth Controls Fault Orientation in Quasibrittle Compressive Failure, *Phys. Rev. Lett.*, 122, 085 501, <https://doi.org/10.1103/PhysRevLett.122.085501>, <https://link.aps.org/doi/10.1103/PhysRevLett.122.085501>, 2019.
- Divine, D. V., Korsnes, R., and Makshtas, A. P.: Temporal and spatial variation of shore-fast ice in the Kara Sea, *Continental Shelf Research*, 24, 1717–1736, <https://doi.org/10.1016/j.csr.2004.05.010>, <http://linkinghub.elsevier.com/retrieve/pii/S0278434304001487>, 2004.
- Dumont, D., Gratton, Y., and Arbetter, T. E.: Modeling the Dynamics of the North Water Polynya Ice Bridge, *Journal of Physical Oceanography*, 39, 1448–1461, <https://doi.org/10.1175/2008JPO3965.1>, 2008.
- Dumont, D., Gratton, Y., and Arbetter, T. E.: Modeling Wind-Driven Circulation and Landfast Ice-Edge Processes during Polynya Events in Northern Baffin Bay, *Journal of Physical Oceanography*, 40, 1356–1372, <https://doi.org/10.1175/2010JPO4292.1>, 2010.
- Girard, L., Bouillon, S., Weiss, J., Amitrano, D., Fichet, T., and Legat, V.: A new modeling framework for sea-ice mechanics based on elasto-brittle rheology, *Annals of Glaciology*, 52, 123–132, <https://doi.org/10.3189/172756411795931499>, 2011.
- Hannah, C. G., Dupont, F., and Dunphy, M.: Polynyas and Tidal Currents in the Canadian Arctic Archipelago, *Arctic*, 62, 83–95, <https://doi.org/10.14430/arctic115>, <https://doi.org/10.14430/arctic115>, 2009.
- Hata, Y. and Tremblay, L. B.: A 1.5-D anisotropic sigma-coordinate thermal stress model of landlocked sea ice in the Canadian Arctic Archipelago, *Journal of Geophysical Research: Oceans*, 120, 8251–8269, <https://doi.org/10.1002/2015JC010820>.Received, 2015a.
- Hata, Y. and Tremblay, L. B.: Anisotropic internal thermal stress in sea ice from the Canadian Arctic Archipelago, *Journal of Geophysical Research: Oceans*, 120, 5457–5472, <https://doi.org/10.1002/2015JC010819>.Received, 2015b.
- Hibler, W., Hutchings, J., and Ip, C.: Sea-ice arching and multiple flow States of Arctic pack ice, *Annals of Glaciology*, 44, 339–344, <https://doi.org/10.3189/172756406781811448>, 2006.
- Hibler, W. D.: A dynamic thermodynamic sea ice model, *Journal of Physical Oceanography*, 9, 815–846, 1979.
- Hunke, E. C.: Viscous–Plastic Sea Ice Dynamics with the EVP Model: Linearization Issues, *Journal of Computational Physics*, 170, 18 – 38, <https://doi.org/https://doi.org/10.1006/jcph.2001.6710>, <http://www.sciencedirect.com/science/article/pii/S0021999101967105>, 2001.
- Hunke, E. C. and Dukowicz, J.: An Elastic – Viscous – Plastic Model for Sea Ice Dynamics, *Journal of Physical Oceanography*, 27, 1849–1867, 1997.
- Ip, C. F.: Numerical investigation of different rheologies on sea-ice dynamics, PhD thesis, 1, 242 pp., 1993.
- Kozo, T. L.: The hybrid polynya at the northern end of Nares Strait, *Geophysical Research Letters*, 18, 2059–2062, <https://doi.org/10.1029/91GL02574>, <https://agupubs.onlinelibrary.wiley.com/doi/abs/10.1029/91GL02574>, 1991.
- Kubat, I., Sayed, M., Savage, S., and Carrieres, T.: Flow of Ice Through Converging Channels, *International Journal of Offshore and Polar Engineering*, 16, 268–273, 2006.

- Kwok, R.: Variability of Nares Strait ice flux, *Geophysical Research Letters*, 32, <https://doi.org/10.1029/2005GL024768>, <https://agupubs.onlinelibrary.wiley.com/doi/abs/10.1029/2005GL024768>, 2005.
- 915 Kwok, R. and Cunningham, G. F.: Contribution of melt in the Beaufort Sea to the decline in Arctic multiyear sea ice coverage: 1993-2009, *Geophysical Research Letters*, 37, n/a–n/a, <https://doi.org/10.1029/2010GL044678>, <http://doi.wiley.com/10.1029/2010GL044678>, 2010.
- Langleben, M.: Young's modulus for sea ice, *Canadian Journal of Physics*, 40, 1–8, 1962.
- Lemieux, J.-F., Tremblay, B., Thomas, S., Sedláček, J., and Mysak, L. A.: Using the preconditioned Generalized Minimum RESidual (GMRES) method to solve the sea-ice momentum equation, *Journal of Geophysical Research*, 113, C10004, 920 <https://doi.org/10.1029/2007JC004680>, 2008.
- Lemieux, J.-f., Knoll, D. A., Losch, M., and Girard, C.: A second-order accurate in time IMPLICIT – EXPLICIT (IMEX) integration scheme for sea ice dynamics, *Journal of Computational Physics*, 263, 375–392, <https://doi.org/10.1016/j.jcp.2014.01.010>, <http://dx.doi.org/10.1016/j.jcp.2014.01.010>, 2014.
- Lemieux, J.-F., Dupont, F., Blain, P., Roy, F., Smith, G. C., and Flato, G. M.: Improving the simulation of landfast ice 925 by combining tensile strength and a parameterization for grounded ridges, *Journal of Geophysical Research: Oceans*, 121, <https://doi.org/10.1002/2016JC012006>, 2016.
- Lemieux, J.-F., Lei, J., Dupont, F., Roy, F., Losch, M., Lique, C., and Laliberté, F.: The Impact of Tides on Simulated Landfast Ice in a Pan-Arctic Ice-Ocean Model, *Journal of Geophysical Research: Oceans*, 123, 1–16, <https://doi.org/10.1029/2018JC014080>, <http://doi.org/10.1029/2018JC014080>, 2018.
- 930 Lewis, J. K.: A model for thermally-induced stresses in multi-year sea ice, *Cold Regions Science and Technology*, 21, 337–348, 1993.
- Losch, M., Menemenlis, D., Campin, J.-M., Heimbach, P., and Hill, C.: On the formulation of sea-ice models. Part 1: Effects of different solver implementations and parameterizations, *Ocean Modelling*, 33, 129 – 144, <https://doi.org/https://doi.org/10.1016/j.ocemod.2009.12.008>, <http://www.sciencedirect.com/science/article/pii/S1463500309002418>, 2010.
- 935 Mahoney, A., Eicken, H., Gaylord, A. G., and Shapiro, L.: Alaska landfast sea ice: Links with bathymetry and atmospheric circulation, *Journal of Geophysical Research*, 112, C02001, <https://doi.org/10.1029/2006JC003559>, <http://doi.wiley.com/10.1029/2006JC003559>, 2007.
- Mahoney, A. R., Eicken, H., Gaylord, A. G., and Gens, R.: Landfast sea ice extent in the Chukchi and Beaufort Seas: The annual cycle and decadal variability, *Cold Regions Science and Technology*, <https://doi.org/10.1016/j.coldregions.2014.03.003>, <http://linkinghub.elsevier.com/retrieve/pii/S0165232X14000585>, 2014.
- 940 Marko, J. R. and Thomson, R. E.: Rectilinear leads and internal motions in the ice pack of the western Arctic Ocean, *Journal of Geophysical Research (1896-1977)*, 82, 979–987, <https://doi.org/10.1029/JC082i006p00979>, <https://agupubs.onlinelibrary.wiley.com/doi/abs/10.1029/JC082i006p00979>, 1977.

- McPhee, M. G.: The effect of the oceanic boundary layer on the mean drift of pack ice: application of a simple model, *Journal of Physical Oceanography*, 9, 388–400, 1979.
- 945 Melling, H.: Sea ice of the northern Canadian Arctic Archipelago, *Journal of Geophysical Research*, 107, 3181, <https://doi.org/10.1029/2001JC001102>, <http://doi.wiley.com/10.1029/2001JC001102>, 2002.
- Moore, G. W. K. and McNeil, K.: The Early Collapse of the 2017 Lincoln Sea Ice Arch in Response to Anomalous Sea Ice and Wind Forcing, *Geophysical Research Letters*, 45, 8343–8351, <https://doi.org/10.1029/2018GL078428>, <https://agupubs.onlinelibrary.wiley.com/doi/abs/10.1029/2018GL078428>, 2018.
- 950 Olason, E.: A dynamical model of Kara Sea land-fast ice, *Journal of Geophysical Research: Oceans*, 121, 3141–3158, <https://doi.org/10.1002/2016JC011638>, <https://agupubs.onlinelibrary.wiley.com/doi/abs/10.1002/2016JC011638>, 2016.
- Pritchard, R. S.: Mathematical characteristics of sea ice dynamics models, *Journal of Geophysical Research: Oceans*, 93, 15 609–15 618, <https://doi.org/10.1029/JC093iC12p15609>, <https://agupubs.onlinelibrary.wiley.com/doi/abs/10.1029/JC093iC12p15609>, 1988.
- Rampal, P., Bouillon, S., Ólason, E., and Morlighem, M.: neXtSIM: a new Lagrangian sea ice model, *The Cryosphere*, 10, 1055–1073, 955 <https://doi.org/10.5194/tc-10-1055-2016>, <https://www.the-cryosphere.net/10/1055/2016/>, 2016.
- Rampal, P., Dansereau, V., Olason, E., Bouillon, S., Williams, T., and Samaké, A.: On the multi-fractal scaling properties of sea ice deformation, *The Cryosphere Discussions*, 2019, 1–45, <https://doi.org/10.5194/tc-2018-290>, <https://www.the-cryosphere-discuss.net/tc-2018-290/>, 2019.
- Rasmussen, T., Nicolai, K., and Kaas, E.: Modelling the sea ice in the Nares Strait, *Ocean Modelling*, 35, 161–172, 960 <https://doi.org/10.1016/j.ocemod.2010.07.003>, 2010.
- Reimnitz, E., Toimil, L., and Barnes, P.: Arctic continental shelf morphology related to sea-ice zonation, Beaufort Sea, Alaska, *Marine Geology*, 28, 179–210, 1978.
- Rice, J. R.: *Solid Mechanics*, Harvard University 2010, 2010.
- Richter-Menge, J. A. and Elder, B.: Characteristics of pack ice stress in the Alaskan Beaufort Sea, *Journal of Geophysical Research*, 103, 965 21 817–21 829, 1998.
- Richter-Menge, J. A., McNutt, S. L., Overland, J. E., and Kwok, R.: Relating arctic pack ice stress and deformation under winter conditions, *Journal of Geophysical Research: Oceans*, 107, SHE 15–1–SHE 15–13, <https://doi.org/10.1029/2000JC000477>, <https://agupubs.onlinelibrary.wiley.com/doi/abs/10.1029/2000JC000477>, 2002.
- Ringeisen, D., Losch, M., Tremblay, L. B., and Hutter, N.: Simulating intersection angles between conjugate faults in sea ice with different 970 viscous–plastic rheologies, *The Cryosphere*, 13, 1167–1186, <https://doi.org/10.5194/tc-13-1167-2019>, <https://www.the-cryosphere.net/13/1167/2019/>, 2019.

- Ryan, P. A. and Münchow, A.: Sea ice draft observations in Nares Strait from 2003 to 2012, *Journal of Geophysical Research: Oceans*, 122, 3057–3080, <https://doi.org/10.1002/2016JC011966>, <https://agupubs.onlinelibrary.wiley.com/doi/abs/10.1002/2016JC011966>, 2017.
- 975 Samelson, R., Agnew, T., Melling, H., and Münchow, A.: Evidence for atmospheric control of sea-ice motion through Nares Strait, *Geophysical Research Letters*, 33, <https://doi.org/10.1029/2005GL025016>, 2006.
- Schreyer, H. L., Sulsky, D. L., Munday, L. B., Coon, M. D., and Kwok, R.: Elastic-decohesive constitutive model for sea ice, *Journal of Geophysical Research: Oceans*, 111, C11S26, <https://doi.org/10.1029/2005JC003334>, 2006.
- Schulson, E. M., Fortt, a. L., Iliescu, D., and Renshaw, C. E.: Failure envelope of first-year Arctic sea ice: The role of friction in compressive fracture, *Journal of Geophysical Research: Oceans*, 111, C11S25, <https://doi.org/10.1029/2005JC003235>, 2006.
- 980 Selyuzhenok, V., Krumpen, T., Mahoney, A., Janout, M., and Gerdes, R.: Seasonal and interannual variability of fast ice extent in the southeastern Laptev Sea between 1999 and 2013, *Journal of Geophysical Research: Oceans*, 120, 7791–7806, <https://doi.org/10.1002/2015JC011135>. Received, 2015.
- Selyuzhenok, V., Mahoney, A., Krumpen, T., Castellani, G., and Gerdes, R.: Mechanisms of fast-ice development in the south-eastern Laptev Sea: a case study for winter of 2007/08 and 2009/10, *Polar Research*, 36, 1411–1440, <https://doi.org/10.1080/17518369.2017.1411140>, 2017.
- 985 <https://doi.org/10.1080/17518369.2017.1411140>, 2017.
- Shroyer, E. L., Samelson, R. M., Padman, L., and Münchow, A.: Modeled ocean circulation in Nares Strait and its dependence on landfast-ice cover, *Journal of Geophysical Research: Oceans*, 120, 7934–7959, <https://doi.org/10.1002/2015JC011091>, <https://agupubs.onlinelibrary.wiley.com/doi/abs/10.1002/2015JC011091>, 2015.
- Sodhi, D. S.: Ice arching and the drift of pack ice through restricted channels, *Cold Regions Research and Engineering Laboratory (CRREL)* Rep. 77-18, p. 11 pp., 1997.
- 990 Rep. 77-18, p. 11 pp., 1997.
- Sukhorukov, K.: Experimental investigations of relaxation properties of sea ice internal stresses, in: *The proceedings of the sixth (1996) international offshore and polar engineering conference*, pp. 354–361, 1996.
- Sulsky, D. and Peterson, K.: Toward a new elastic – decohesive model of Arctic sea ice, *Physica D Nonlinear Phenomena*, 240, 1674–1683, <https://doi.org/10.1016/j.physd.2011.07.005>, 2011.
- 995 <https://doi.org/10.1016/j.physd.2011.07.005>, 2011.
- Tabata, T.: A measurement of Visco-Elastic Constants of Sea Ice, *Journal of the Oceanographical Society of Japan*, 11, 185–189, 1955.
- Tang, C.: Numerical simulation of progressive rock failure and associated seismicity, *International Journal of Rock Mechanics and Mining Sciences*, 34, 249 – 261, [https://doi.org/https://doi.org/10.1016/S0148-9062\(96\)00039-3](https://doi.org/https://doi.org/10.1016/S0148-9062(96)00039-3), <http://www.sciencedirect.com/science/article/pii/S0148906296000393>, 1997.
- Timco, G. W. and Weeks, W. F.: A review of the engineering properties of sea ice, *Cold Regions Science and Technology*, 60, 107–129, <https://doi.org/10.1016/j.coldregions.2009.10.003>, <http://dx.doi.org/10.1016/j.coldregions.2009.10.003>, 2010.
- 1000 <https://doi.org/10.1016/j.coldregions.2009.10.003>, 2010.

- Tran, H. D., Sulsky, D. L., and Schreyer, H. L.: An anisotropic elastic-decohesive constitutive relation for sea ice, *International Journal for Numerical and Analytical Methods in Geomechanics*, 39, 988–1013, <https://doi.org/10.1002/nag>, 2015.
- Tremblay, L.-B. and Hakakian, M.: Estimating the Sea Ice Compressive Strength from Satellite-Derived Sea Ice Drift and NCEP Reanalysis Data, *Journal of Physical Oceanography*, 36, 2165–2172, 2006.
- 1005 Tremblay, L.-B. and Mysak, L. A.: Modeling Sea Ice as a Granular Material , Including the Dilatancy Effect, *Journal of Physical Oceanography*, 27, 2342–2360, 1997.
- Tucker, W. B. and Perovich, D. K.: Stress measurements in drifting pack ice, *Cold Regions Science and Technology*, 20, 119–139, 1992.
- Turnbull, I. D., Torbati, R. Z., and Taylor, R. S.: Relative influences of the metocean forcings on the drifting ice pack and estimation of internal ice stress gradients in the Labrador Sea, *Journal of Geophysical Research: Oceans*, 122, 5970–5997, 1010 <https://doi.org/10.1002/2017JC012805>, <https://agupubs.onlinelibrary.wiley.com/doi/abs/10.1002/2017JC012805>, 2017.
- Vincent, R. F.: A Study of the North Water Polynya Ice Arch using Four Decades of Satellite Data, *Scientific Reports*, 9, 20278, <https://doi.org/10.1038/s41598-019-56780-6>, <https://doi.org/10.1038/s41598-019-56780-6>, 2019.
- Wang, K.: Observing the yield curve of compacted pack ice, *Journal of Geophysical Research: Oceans*, 112, <https://doi.org/10.1029/2006JC003610>, <https://agupubs.onlinelibrary.wiley.com/doi/abs/10.1029/2006JC003610>, 2007.
- 1015 Weeks, W. F. and Assur, A.: The mechanical properties of sea ice, *Cold Regions Science and Engineering*, II, 1967.
- Weiss, J., Schulson, E. M., and Stern, H. L.: Sea ice rheology from in-situ , satellite and laboratory observations : Fracture and friction, *Earth and Planetary Science Letters*, 255, 1–8, <https://doi.org/10.1016/j.epsl.2006.11.033>, 2007.
- Wilchinsky, A. V. and Feltham, D. L.: A continuum anisotropic model of sea-ice dynamics, *Proceedings of the Royal Society of London. Series A: Mathematical, Physical and Engineering Sciences*, 460, 2105–2140, <https://doi.org/10.1098/rspa.2004.1282>, <https://royalsocietypublishing.org/doi/abs/10.1098/rspa.2004.1282>, 1020 <https://royalsocietypublishing.org/doi/abs/10.1098/rspa.2004.1282>, 2004.
- Williams, J., Tremblay, L. B., and Lemieux, J.-f.: The effects of plastic waves on the numerical convergence of the viscous – plastic and elastic – viscous – plastic sea-ice models, *Journal of Computational Physics*, 340, 519–533, <https://doi.org/10.1016/j.jcp.2017.03.048>, <http://dx.doi.org/10.1016/j.jcp.2017.03.048>, 2017.
- Yu, Y., Stern, H., Fowler, C., Fetterer, F., and Maslanik, J.: Interannual Variability of Arctic Landfast Ice between 1976 and 2007, *Journal of* 1025 *Climate*, 27, 227–243, <https://doi.org/10.1175/JCLI-D-13-00178.1>, 2014.
- Zhang, J. and Hibler, W. D.: On an efficient numerical method for modeling sea ice dynamics, *Journal of Geophysical Research*, 102, 8691–8702, 1997.

Table 1. Material strength parameters from observations

Parameter	Reference	Parameter	Value
Young Modulus	Langleben (1962)	E	6.5–10 GPa <u>6.5–10 GN m⁻²</u>
	Weeks and Assur (1967)		1–9 GPa <u>1–9 GN m⁻²</u>
	Tabata (1955)		7–18 GPa <u>7–18 GN m⁻²</u>
Poisson ratio	Weeks and Assur (1967)	ν	0.33 - 0.4
Viscosity	Tabata (1955)	η_0	$0.6 - 2.4 \times 10^{12} \text{ kgm}^{-1}\text{s}^{-1}$
Viscous relaxation time	Tabata (1955) ^a	λ_0	14 – 40 min
	Weeks and Assur (1967) ^a		28 – 32 min
	Sukhorukov (1996) ^a		66 h
	Hata and Tremblay (2015b)		10 ⁵ s
Angle of internal friction	Schulson et al. (2006)	ϕ	~ 42°
	Weiss et al. (2007)		~ 44°
Compressive strength	Weiss et al. (2007)	σ_c	50 kPa <u>50 kN m⁻²</u>
	Tremblay and Hakakian (2006) ^b		30 - 100 kPa <u>kN m⁻²</u>
	Tucker and Perovich (1992) ^c		30 kPa <u>kN m⁻²</u>
	Richter-Menge et al. (2002) ^c		30–50 kPa <u>30–50 kN m⁻²</u>
	Richter-Menge and Elder (1998) ^c		100–200 kPa <u>kN m⁻²</u>
Tensile strength	Weiss et al. (2007)	σ_t	50 kPa <u>50 kN m⁻²</u>
	Tremblay and Hakakian (2006) ^b		25–30 kPa <u>kN m⁻²</u>
	Tucker and Perovich (1992) ^c		30 kPa <u>kN m⁻²</u>
	Richter-Menge and Elder (1998) ^c		50 kPa <u>kN m⁻²</u>
Cohesion	<u>Sodhi (1997)^b</u>	c_0	<u>1.99 N m⁻¹</u>
	Weiss et al. (2007)	e	40 kPa <u>40 kN m⁻²</u>

^a From small scale measurements in the field.

^b Estimate from satellite observations.

^c Observed peak stresses.

Table 2. Default Model Parameters

Parameter	Definition	Value
Δx	Spatial resolution	2 km <u>km</u>
Δt	Time step	2 s <u>0.5 s</u>
T_d	Damage time scale	2 s
Y	Young Modulus	1 GPa <u>1 GN m⁻²</u>
ν	Poisson ratio	0.3 <u>0.3</u>
λ_0	Viscous relaxation time	10⁷ s <u>10⁵ s</u>
ϕ	Angle of internal friction	45° <u>45°</u>
c <u>c_0</u>	Cohesion	20 kN/m <u>10 kN m⁻²</u>
σ_t <u>σ_{ca}</u>	Isotropic tensile strength <u>28 kN/m</u> σ_c Isotropic-compressive strength	50 kN/m <u>50 kN m⁻²</u>
ρ_a	Air density	1.3 kg/m³ <u>1.3 kgm⁻³</u>
ρ_i	Sea ice density	9.0 × 10² kg/m³ <u>9.0 × 10² kgm⁻³</u>
ρ_w	Sea water density	1.026 × 10³ kg/m³ <u>1.026 × 10³ kgm⁻³</u>
C_{da}	Air drag coefficient	1.2 × 10 ⁻³
C_{dw}	Water drag coefficient	5.5 × 10 ⁻³

Table 3. Material properties used in sea ice models (VP,EVP and MEB)

Parameter	Reference	Parameter	Value
Young Modulus	Hunke (2001) Hunke (2001)	$E = \zeta/T$	1060 GPa 1060 GN m⁻²
	Bouillon and Rampal (2015)	Y	9 GPa 9 GN m⁻²
	Dansereau et al. (2016)	E_0	0.585 GPa 0.585 GN m⁻²
	Sulsky and Peterson (2011)	E	1 MPa 1 MN m⁻²
	Tran et al. (2015)	E	1 MPa 1 MN m⁻²
Maximum Viscosity	Olason (2016)	ζ_{max}	378×10^{15} kg/s 378×10^{15} kg s⁻¹
	Dansereau et al. (2016) ^a	$\eta_0 = 10^7 E_0$	5.85×10^{15} kg/ms 5.85×10^{15} kg m⁻¹ s⁻¹
	Hunke (2001) Hunke (2001)	ζ_{max}	1375×10^{12} kg/s 1375×10^{12} kg s⁻¹
	Tremblay and Mysak (1997)	η_{max}	1×10^{12} kg/s 1×10^{12} kg s⁻¹
	Hibler (1979)	ζ_{max}	125×10^9 kg/s 125×10^9 kg s⁻¹
	Dumont et al. (2008)	ζ_{max}	4×10^8 kg s⁻¹
Compressive strength	Tran et al. (2015)	f'_c	125 kPa 125 kN m⁻²
	Sulsky and Peterson (2011)	f'_c	125 kPa 125 kN m⁻²
	Lemieux et al. (2016) ^a	P_p	100 kPa 100 kN m⁻²
	Olason (2016)	p^*	40 kPa 40 kN m⁻²
	Dansereau et al. (2016)	σ_c	48 - 96 kPa kN m⁻²
	Hunke (2001) Hunke (2001) ^a	P	27.5×10^4 kPa 27.5×10^4 kN m⁻²
	Dumont et al. (2008)	P^*	27.5 kPa 27.5 kN m⁻²
	Bouillon and Rampal (2015)	$\sigma_{Nmin} = -\frac{5}{2}c$	1.25 - 20 kPa 1.25 - 20 kN m⁻²
	Tremblay and Mysak (1997)	P_{max}	7 kPa kN m⁻²
Hibler (1979)	P^*	5.0 kPa 5.0 kN m⁻²	

Table 3. Table 3 continued

Parameter	Reference	Parameter	Value
Shear strength :	Hibler (1979)	e	2
	Hunke (2001) <u>Hunke (2001)</u>	e	2
	Dumont et al. (2008)	e	1.2 – 1.6
	Lemieux et al. (2016)	e	1.4 – 1.6
	Olason (2016)	e	1.3 – 2.1
	Dansereau et al. (2016)	C	25 - 50 kPa <u>kN m⁻²</u>
	Olason (2016)**	σ_{uc}	16 – 22 kPa <u>16 – 22 kN m⁻²</u>
	Tran et al. (2015)	τ_{sf}	15 – 75 kPa <u>15 – 75 kN m⁻²</u>
	Sulsky and Peterson (2011)	τ_{sf}	15 kPa <u>15 kN m⁻²</u>
Bouillon and Rampal (2015)	c	0.5 – 8 kPa <u>0.5 – 8 kN m⁻²</u>	
Tensile strength	Olason (2016) ^b	Pk_t	3.4 – 5 kPa <u>kN m⁻²</u>
	Lemieux et al. (2016)	$k_t P_p$	10 – 20 kPa <u>kN m⁻²</u>
	Beatty and Holland (2010)	k_t	27.5 kPa <u>kN m⁻²</u>
	Dansereau et al. (2016)	$\sigma_t = 0.27\sigma_c$	12.96 – 25.92 kPa <u>12.96 – 25.92 kN m⁻²</u>
	Tran et al. (2015)	τ_{nf}	25 kPa <u>25 kN m⁻²</u>
	Sulsky and Peterson (2011)	τ_{nf}	25 kPa <u>25 kN m⁻²</u>
	Bouillon and Rampal (2015)	$\sigma_{Nmax} = \frac{5}{4}c$	0.6 – 10 kPa <u>0.6 – 10 kN m⁻²</u>

^afor 1m thick ice

^bUsing the Mohr-Coulomb curve with $\phi = 45^\circ$

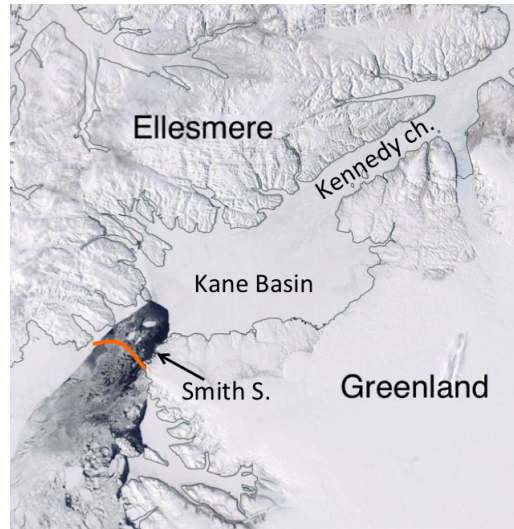


Figure 1. NASA Worldview ~~images-image~~ of a stable landfast ice arches in Nares Strait, from Moderate Resolution Imaging Spectroradiometer (MODIS) Corrected Reflectance imagery (True Color). ~~a) Multiple ice arches in the Northwest Passage region, on June 7th 2018.~~
~~b) Nares Strait ice arch, on~~ May 1st 2018. Orange curves indicate the position of stable ice arches in (Dansereau et al., 2017)

~~Location of the scalars $(C_{i,j})$ and vector components $(u_{i,j}, v_{i,j})$ on the Arakawa C-grid. The normal and shear stress components used in the memory term are located center $(C_{i,j})$ and nodes $(Z_{i,j})$ respectively.~~

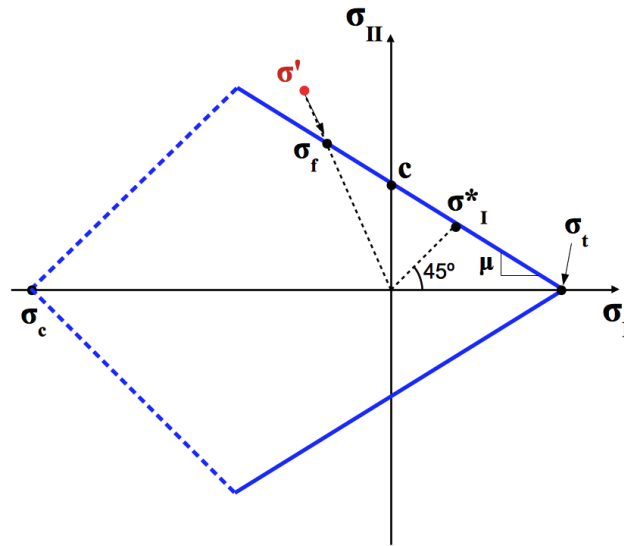


Figure 2. Mohr-Coulomb yield criterion (Mohr-Coulomb and compressive cut-off) in stress invariant space (σ_I, σ_{II}) with the mechanical strength parameters: compressive strength (σ_c), cohesion (c), coefficient of internal friction ($\mu = \sin \phi$, ϕ being the angle of internal friction), isotropic tensile strength (σ_t) and uniaxial-uni-axial tensile strength (σ_I^* , where the second principal stress invariant σ_2 is zero, or $\sigma_I = \sigma_{II} = \sigma_I^*$). The stress before and after the correction (see Eq. 13) is denoted by σ' , and σ_f respectively. The correction from σ' to σ_f is done following a line going through the origin.

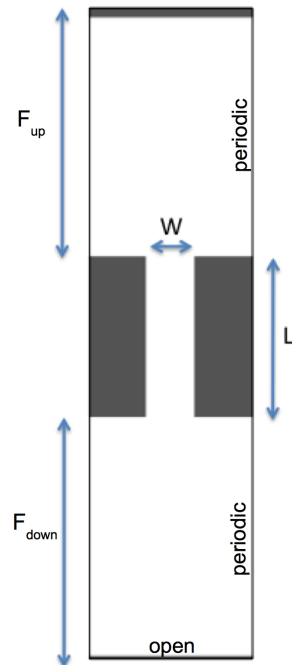


Figure 3. Idealized domain with a solid wall to the north, open boundary to the south and periodic boundaries to the East and West. The channel has a width W , length L and fetch F_{up} and F_{down} in the upwind upstream and downwind downstream basins respectively.

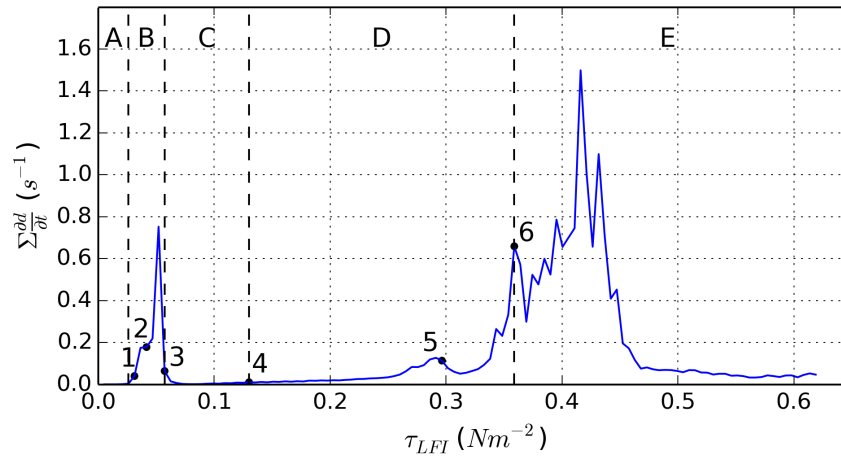


Figure 4. ~~Top panel:~~ Time series of the domain integrated brittle fracture activity ($\partial d/\partial t$) for the control run simulation. Dashed lines indicate the beginning and end of the simulation phases (A,B,C,D,E). ~~Numbers~~, and numbers indicate the location of the damage field in Fig. ~~??~~ 5 and ~~??~~ 6.

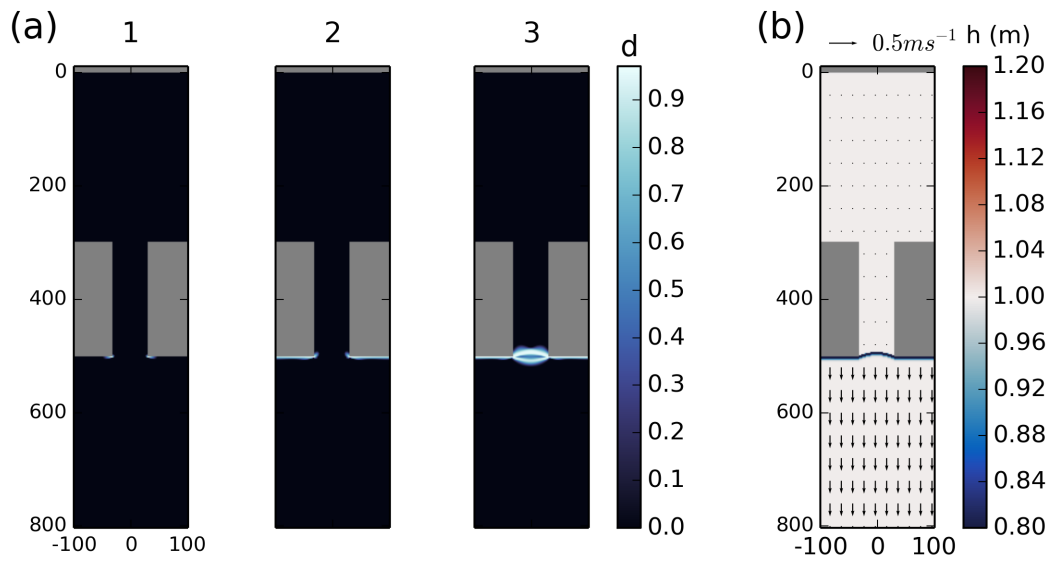


Figure 5. a) Damage field at the surface forcing indicated by points 1, 2 and 3 in Fig. 4, during the formation of the downwind-downstream ice arch, at points indicated in Fig. 4. b) Sea ice thickness and drift following the formation of the downwind-downstream ice arch, while the ice bridge remains stable (Phase C)

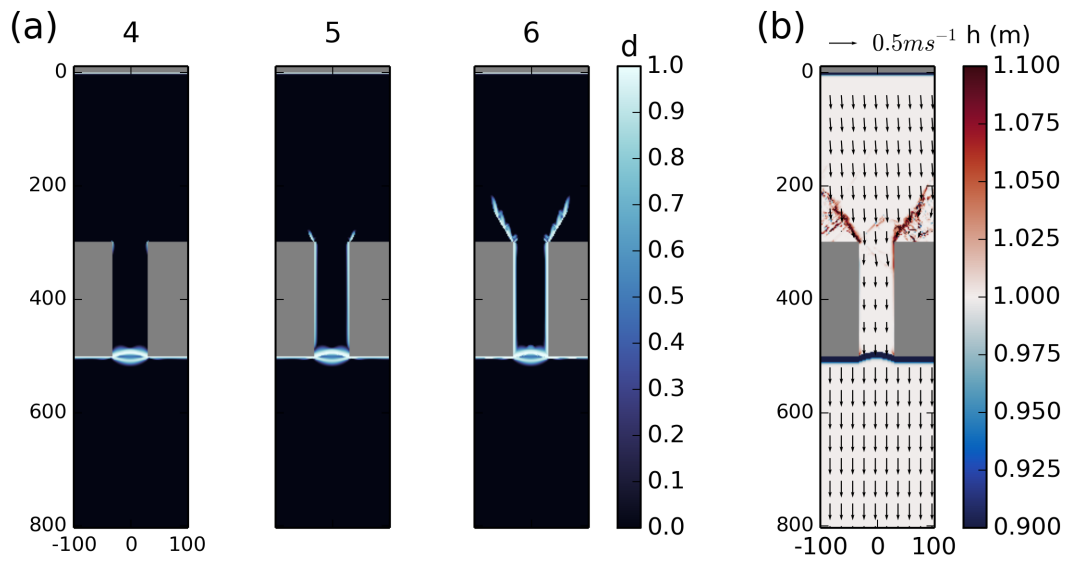


Figure 6. a) Damage field at the surface forcing indicated by points 4, 5 and 6 in Fig. 4, during ice-the formation of upwind-the upstream lines of fracture, at points indicated in Fig. 4. b) Sea ice thickness and drift following the ice bridge collapse (Phase E).

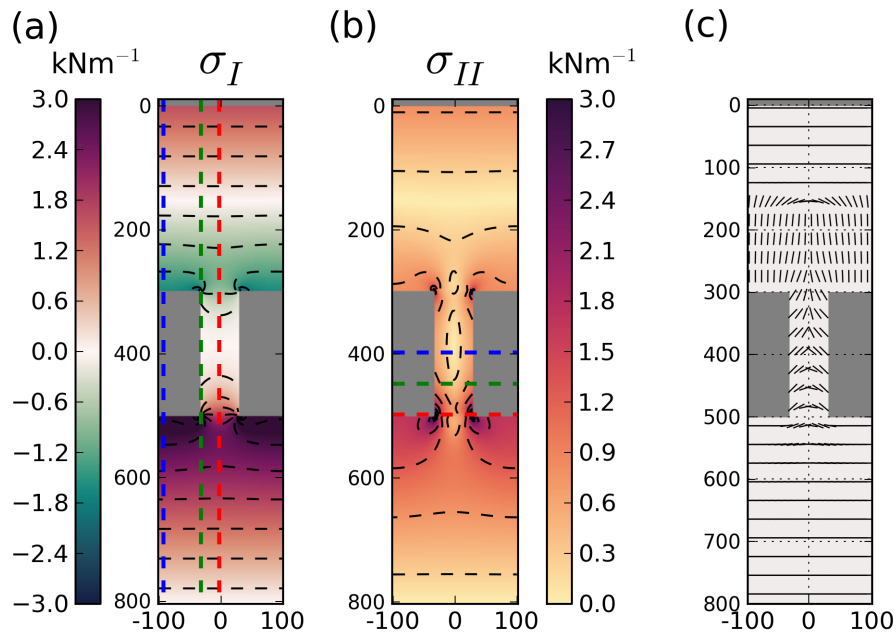


Figure 7. Stress fields in landfast ice during Phase A. a) Normal stress invariant (σ_I), with colored dashed lines to indicate the vertical transects used in Fig. 8, b) shear stress invariant (σ_{II}), with colored lines to indicate the vertical transects used in Fig. 8, c) orientation of the second principal stress componantcomponent.

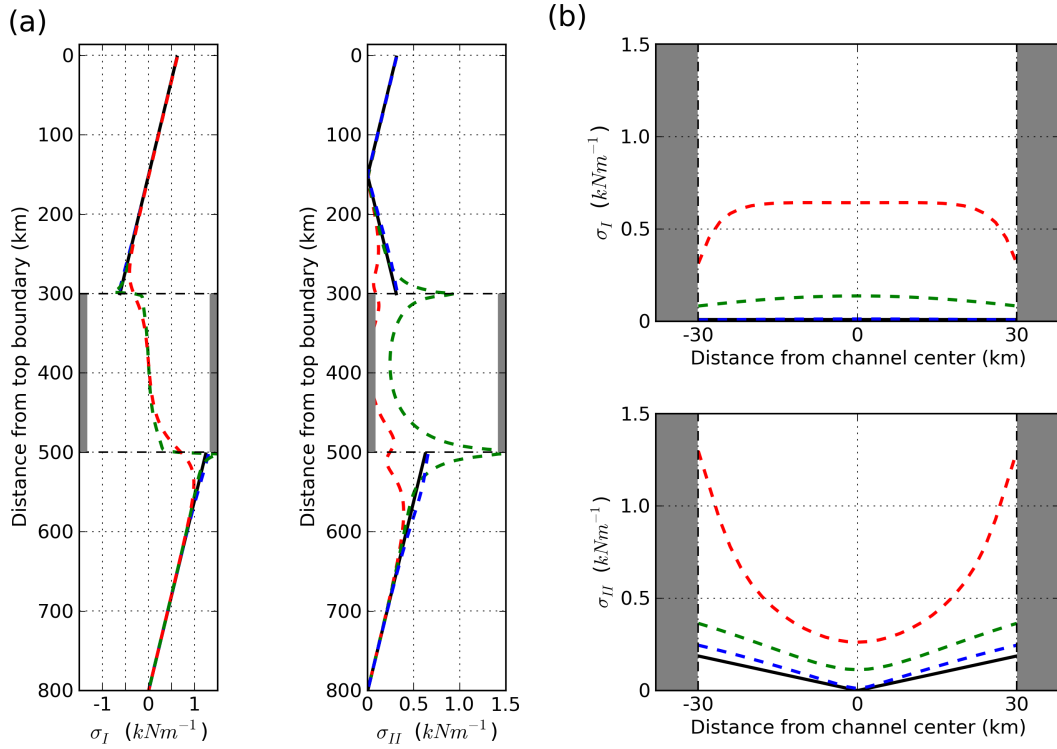


Figure 8. Stress invariants (σ_I , σ_{II}) along the transects of corresponding colors in Fig. 7: a) transects running along the y-direction and b) transects running along the x-direction. Black solid lines indicate the analytic solutions. Grey area indicate the position of the islands.

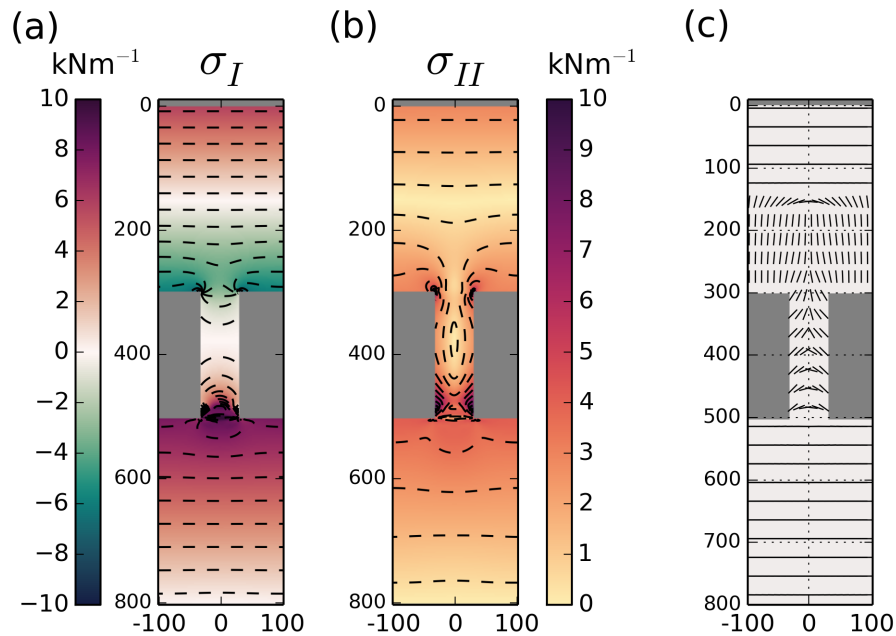


Figure 9. Stress fields during Phase C. a) Normal stress invariant (σ_I), with colored lines to indicate the vertical transects used in Fig. 8, b) shear stress invariant (σ_{II}), with colored lines to indicate the vertical transects used in Fig. 8, c) orientation of the second principal stress component.

1030 Left: Location of four points associated to the first fracture in the domain (red), the center of the ice arch (orange), the fracture at the upstream channel corners (green) and along the upstream shear fracture line (blue). Right : stress state and orientation of the strain rate tensor at the 4 indicated points they reach the yield curve. The Mohr Coulomb criterion is in black. Colored line indicate the path of the stress state at each points prior to the fracture.

a) Damage field during ice formation of upwind lines of fracture, at points indicated in Fig. 4. b) Sea ice thickness and drift following the ice bridge collapse (Phase E)

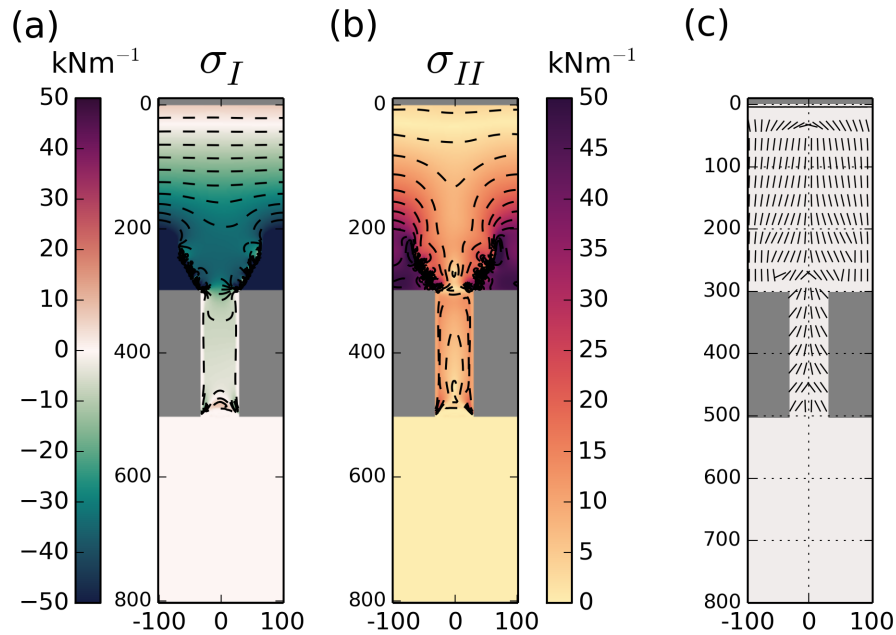


Figure 10. Stress fields during Phase E. a) Normal stress invariant (σ_I), with colored lines to indicate the vertical transects used in Fig. 8, b) shear stress invariant (σ_{II}), with colored lines to indicate the vertical transects used in Fig. 8, c) orientation of the second principal stress component.

Damage fields during Phase E for different solution residual tolerance. Left: $\epsilon_{res} = 10^{-6}$, right: $\epsilon_{res} = 10^{-10}$

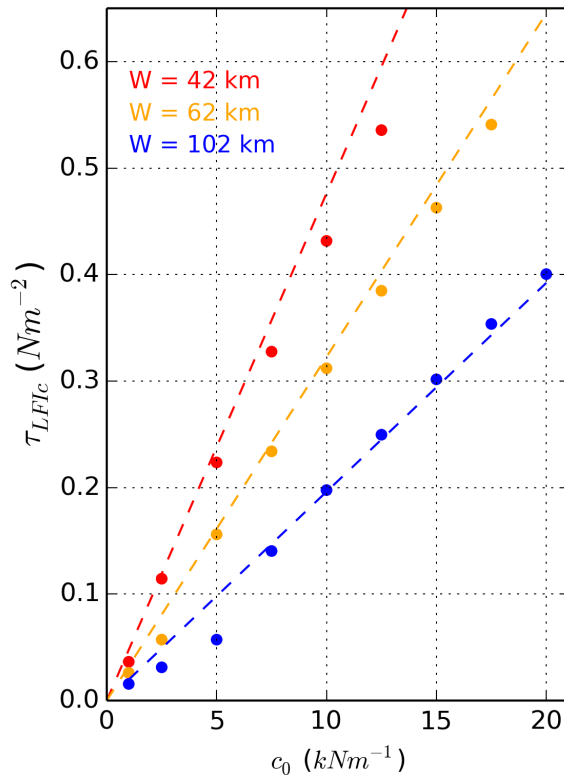


Figure 11. Critical wind surface forcing associated with the second fracture event (stage D) as a function of cohesion and channel width (dots). The graph on Dashed lines indicate the right shows analytic solution from the slope between the critical forcing and the cohesion as a function of the channel width 1D equations.

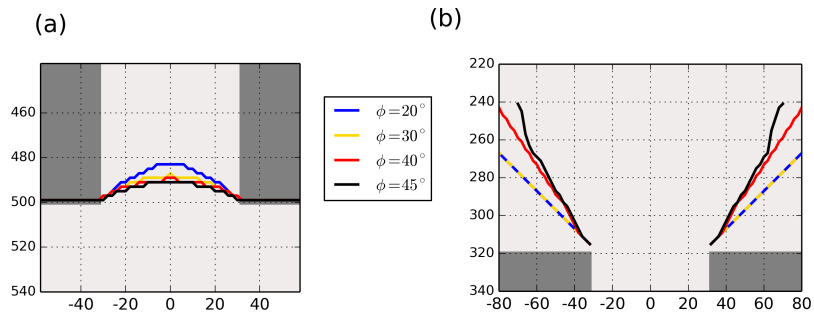


Figure 12. Shape of the lines of fracture using different angles of internal friction: a) for the downwind-downstream ice arches and b) for the upwind-upstream lines of fracture (the green-yellow and blue-purple lines are superposed).

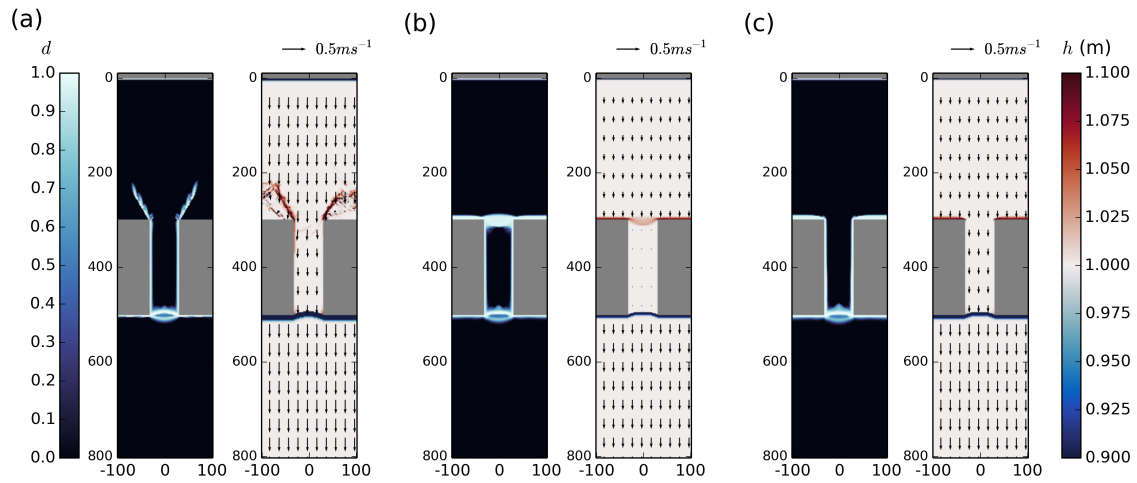


Figure 13. Spatial distribution of the damage field at the end of stage D (left) and the sea ice thickness and velocity fields at the end of the simulation (right). For different compressive strength criterion: a) $\sigma_c = 5.0$ $\sigma_{c0} = 5.0$ kN /m⁻¹, b) with $\sigma_c = 25.0$ $\sigma_{c0} = 25.0$ kN /m⁻¹ and c) with $\sigma_c = 100.0$ $\sigma_{c0} = 100.0$ kN /m⁻¹.

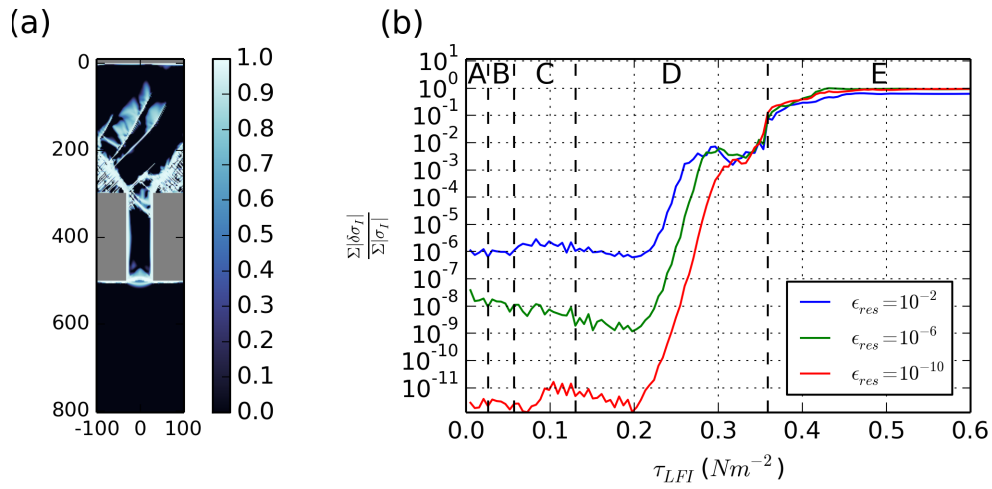


Figure 14. a) Asymmetries dominating the damage fields after the ice bridge collapse (Stage E) in Fig. 4. b) Evolution of normalized, domain-integrated asymmetries in the σ_I field when using different residual tolerance ϵ_{res} on the solution. Dashed lines indicate the beginning and end of the simulation phases (A,B,C,D,E).